

Full Paper

Round Granules of Dimethyl Fumarate by Three-in-One Intensified Process of Reaction, Crystallization and Spherical Agglomeration in a Common Stirred Tank

Chih Wei Chen, and Tu Lee

Org. Process Res. Dev., **Just Accepted Manuscript** • DOI: 10.1021/acs.oprd.7b00183 • Publication Date (Web): 31 Jul 2017Downloaded from <http://pubs.acs.org> on July 31, 2017

Just Accepted

“Just Accepted” manuscripts have been peer-reviewed and accepted for publication. They are posted online prior to technical editing, formatting for publication and author proofing. The American Chemical Society provides “Just Accepted” as a free service to the research community to expedite the dissemination of scientific material as soon as possible after acceptance. “Just Accepted” manuscripts appear in full in PDF format accompanied by an HTML abstract. “Just Accepted” manuscripts have been fully peer reviewed, but should not be considered the official version of record. They are accessible to all readers and citable by the Digital Object Identifier (DOI®). “Just Accepted” is an optional service offered to authors. Therefore, the “Just Accepted” Web site may not include all articles that will be published in the journal. After a manuscript is technically edited and formatted, it will be removed from the “Just Accepted” Web site and published as an ASAP article. Note that technical editing may introduce minor changes to the manuscript text and/or graphics which could affect content, and all legal disclaimers and ethical guidelines that apply to the journal pertain. ACS cannot be held responsible for errors or consequences arising from the use of information contained in these “Just Accepted” manuscripts.



1
2
3
4 Round Granules of Dimethyl Fumarate by Three-in-One
5
6 Intensified Process of Reaction, Crystallization and Spherical
7
8
9
10 Agglomeration in a Common Stirred Tank
11
12
13
14
15
16

17 Chih Wei Chen and Tu Lee*

18 Department of Chemical and Materials Engineering, National Central University,
19

20 300 Jhongda Road, Jhongli District, Taoyuan City 32001, Taiwan R.O.C.
21
22
23
24
25
26

27 **ABSTRACT**
28
29

30 Pure, isomorphic, round and free-flowing dimethyl fumarate granules in a size
31
32 range of 250 to 2000 μm were successfully produced directly from esterification
33
34 through the three-in-one intensified process of three distinctive steps of reaction,
35
36 crystallization and spherical agglomeration (SA) in a 0.5 L-sized jacketed glass stirred
37
38 tank. Dimethyl fumarate was prepared by sulfuric acid-catalyzed esterification of
39
40 fumaric acid with methanol. The reaction temperature was below the maximum
41
42 allowable limit of 65°C as determined by reaction kinetics to avoid runaway situation.
43
44
45
46
47
48
49
50 The dissolution rate of primary crystals of dimethyl fumarate was inversely
51
52 proportional to the particle size which was strongly affected by the antisolvent
53
54
55

56 * Corresponding Author
57 Phone: +886-3-422-7151 ext. 34204. Fax: + 886-3-425-2296.
58 E-mail: tulee@cc.ncu.edu.tw.
59
60

1
2
3
4 addition and temperature cooling schemes during crystallization. However, the
5
6
7 dissolution rate of the round granules was mainly dependent on the exterior dimension
8
9
10 of the granules and not so much on the primary crystal size inside the granules. The
11
12
13 mechanical properties such as density, porosity Carr's index, friability and fracture
14
15
16 force of round dimethyl fumarate granules generated in: (1) three-in-one processes
17
18
19 with the final temperatures at either 5°C or 25°C (Three-in-one I and II), and (2) SA of
20
21
22 dimethyl fumarate was done separately and disconnected from the train of reaction
23
24
25 and crystallization process at either 5°C or 25°C (SA I and II), were thoroughly
26
27
28 studied and compared. The concept of scale-up for Three-in-one I and II was also
29
30
31 verified in 10 L-sized jacketed glass stirred tank. Powder manufacturability such as
32
33
34 flowability, blend uniformity and compressibility had been substantially enhanced by
35
36
37 spherical agglomeration. The added values of free flowing and easy-to-pack
38
39
40 properties to dimethyl fumarate in addition to its original intrinsic slip planes in the
41
42
43 crystal lattice would make direct compaction into tablets feasible.
44
45

46 47 **KEYWORDS**

48
49
50 Process Intensification, Dimethyl Fumarate, Reaction, Crystallization, Spherical
51
52
53 Agglomeration
54
55
56
57
58
59
60

INTRODUCTION

Pharmaceutical companies have long competed mainly through the innovation of new drugs for medical needs. However, new biotechnologies and paradigms, such as proteomics, genomics and the use of biomarkers, have made the situation more competitive. Many customized small volume drugs for patients' specific genetic makeup have been generated and translated into manufacturing of many more futuristic products.¹ In addition, the increases in competition and proportion of generic utilization, opening of new markets, and the socioeconomic pressures for price controls, have driven the industry to look for other ways to improve quality while reducing manufacturing costs which account for 36% of the industry's cost.²

One possible solution is continuous processing³ of solid dosage products from the synthesis of active pharmaceutical ingredient (API) to the final packaging of tablets or capsules all year round because of less scale-up difficulties, smaller in equipment size, shorter in residence time, better process control, enhanced margins of safety, increase in production rate (> 50 tons/day), and improved quality and yields.^{4,5} However, the industry as a whole is reluctant to embrace continuous manufacturing because: (1) batch processing equipment in many ways is the most flexible and convenient, and unit operations such as API synthesis, milling, blending, roller compaction, extrusion and compression, are not continuous, (2) the additional capital

1
2
3
4 investment for the current vast disposal of batch process equipment and staff training
5
6 required is enormous, and (3) the particle size distribution (PSD) of the APIs are
7
8 highly process dependent.⁶ A tight control of PSD is critical because it has
9
10 significant effects not only on final drug product performance such as dissolution and
11
12 bioavailability, but also on powder manufacturability such as flowability, blend
13
14 uniformity and compressibility. For example, API particles may suffer from
15
16 troublesome problems in powder processing such as wall adhesion, rat-holing,
17
18 bridging and segregation due to its small size and inhomogeneity. In addition,
19
20 pharmaceutical particles, which usually range in size from 1 to 120 μm , are required
21
22 to mix with other excipients to granulate before tablet compaction or capsule filling,
23
24 and granule size used in solid dosage products often ranges from 0.2 to 4.0 mm.⁷
25
26 The size range of 0.2 to 4.0 mm is hard to be achieved by seeding and milling.
27
28 Therefore, granulation methods such as roller compaction,^{8,9} spray drying,⁹
29
30 supercritical fluid,¹⁰ high shear mixing,^{11, 12} fluid bed granulation,⁹ and
31
32 extrusion/spheronization¹³ have been successful in manufacturing of various
33
34 pharmaceutical solid dosage forms. However, those methods are complicated,
35
36 time-consuming, requiring a large space and many expensive equipment. On the
37
38 other hand, spherical agglomeration (SA)¹⁴⁻¹⁷ is an appealing technique for
39
40 intensifying some of the processes especially when round API granules composed of
41
42
43
44
45
46
47
48
49
50
51
52
53
54
55
56
57
58
59
60

1
2
3
4 small and high-aspect-ratio API crystals can be prepared by SA right after
5
6
7 crystallization in the same stirred tank. The relatively large round API agglomerates
8
9
10 can improve filtration and dryer performance in downstream. Their excellent
11
12
13 flowability will allow them to be blended directly and uniformly with the excipients in
14
15
16 the formulation step as well.

17
18 Therefore, our aims in this project are twofold: to achieve satisfactory powder
19
20
21 flowability of API on one hand, and a reasonable compromise between batch-centered
22
23
24 mentality and process intensification on the other. These can be realized by
25
26
27 immediate preparation of API granules right after chemical reaction and
28
29
30 crystallization with a high purity profile in the same common stirred tank by SA,
31
32
33 so-called “three-in-one intensified process.” In this type of three-in-one intensified
34
35
36 process, filtration and drying steps are needed only once after SA, whereas in the
37
38
39 previous studies on SA,¹⁴⁻¹⁷ without having the chemical reaction of solid materials,
40
41
42 SA had been achieved mainly through re-crystallization. That is, the filtration and
43
44
45 drying steps were carried out twice, one after the chemical reaction and crystallization,
46
47
48 and the second one after SA. Hopefully, some of the downstream activities in
49
50
51 formulation such as granulation used for enhancing particle property will soon to be
52
53
54 reduced by implementing the three-in-one intensified process of reaction,
55
56
57 crystallization and spherical agglomeration.^{5, 18} Its robustness may be readily
58
59
60

1
2
3
4 adopted for contract development and manufacturing organizations (CDMO) and
5
6
7 manufacturing companies in APIs, generic drugs, nutraceuticals and other fine
8
9
10 chemicals whose raw materials are supplied from various sources, and main concerns
11
12
13 are flexibility, capacity optimization and cost reduction for staying competitive and
14
15
16 increasing the market share.

17
18 Taking the API as an example, basic SA involves suspending the API crystals
19
20
21 in a poor solvent and agglomerating them by the addition of bridging liquid. The
22
23
24 bridging liquid is immiscible with the poor solvent, and wets the suspended API
25
26
27 crystals preferentially.¹⁹ When SA is coupled with re-crystallization, the API crystals
28
29
30 are firstly dissolved in a good solvent, crystallized out by adding a poor solvent,²⁰ and
31
32
33 then coagulated by introducing the bridging liquid with polymers.²¹ When SA is
34
35
36 coupled with co-crystallization,²² co-crystallization/re-crystallization and
37
38
39 agglomeration are controlled separately to tailor the crystal size internally and the
40
41
42 agglomerate size externally,¹⁶ and sometimes, with the assistance of excipient
43
44
45 surface.²³ So far, SA has only been implemented to batch,¹⁹ two-stage continuous,¹⁶
46
47
48 continuous,¹⁷ and microfluidic modes,²⁴ and conducted indirectly on crystals
49
50
51 produced from neutralization^{25,26} and solvothermal process²⁷ in separate vessels.
52
53
54 However, SA has not yet been coupled with the train of reaction and crystallization,
55
56
57 such as esterification-crystallization system. Since our research group has had
58
59
60

1
2
3
4 experiences with SA of dimethyl fumarate suspension in a common stirred tank,¹⁹ we
5
6
7 would like to continue with the same system, but this time, promoting the telescopic
8
9
10 concept of integrating chemical reaction, crystallization and SA seamlessly in the
11
12
13 same stirred tank.

14
15 Dimethyl fumarate is chosen as a model API (Tecfidera[®]) because of its
16
17
18 multiple applications in antifungal, antiseptic and antimoist in food industry, and the
19
20
21 treatment of psoriasis, and multiple sclerosis.²⁸ High purity dimethyl fumarate can
22
23
24 also be synthesized easily by esterification of fumaric acid with methanol in the
25
26
27 presence of homogeneous acid catalyst such as sulfuric acid.²⁹ Esterification is an
28
29
30 important but common reaction for making organic solvents, fragrances, flavor
31
32
33 chemicals, agrochemicals and pharmaceuticals. In addition, due to the inherent slip
34
35
36 planes in the crystal lattice of dimethyl fumarate, direct compaction should have been
37
38
39 technically feasible if not because of its undesirable plate-like habit³⁰ which has
40
41
42 prevented the dimethyl fumarate crystals from free-flowing in the tableting machine.
43
44
45 To enhance its manufacturability, dimethyl fumarate crystals would need to be
46
47
48 agglomerated first into round granules. As a first step, small primary crystals will
49
50
51 have to be generated from a high degree of supersaturation to serve as ideal building
52
53
54 blocks. This could be achieved by antisolvent addition such as cold water addition,
55
56
57 and temperature cooling at the end of esterification reaction, to create a large
58
59
60

1
2
3
4 temperature gradient. Therefore, esterification will preferably be carried out at a
5
6
7 high temperature but below the maximum allowable reaction temperature as
8
9
10 determined by the reaction kinetics (Supporting Information) to avoid the runaway
11
12
13 situation due to the low boiling point of the methanol-based reaction medium.³¹
14

15
16 Since a wide range of particle size distribution (PSD) of API can be achieved
17
18 in the crystallization step, and the PSD of API can in turn influence the growth
19
20 mechanism of the round granules in SA, round granules of different sizes will be
21
22 produced³² which are easily filtered and dried. Strategically, the two separate events
23
24 of crystallization and SA can be orchestrated¹⁶ to tune the majority of round granules
25
26 to fall mainly in the range of 250 to 2000 μm at will which is difficult to achieve by
27
28 conventional methods, such as seeding, within a reasonable batch time. The absence
29
30 of filtration and drying steps between the non-stop action of crystallization and SA
31
32 steps during the three-in-one intensified process also allows the favorable production
33
34 of small sized crystals in the crystallization step without worrying that they would
35
36 create any high wet cake resistance in filtration or powder lumping in drying, which
37
38 usually take place after the crystallization step.³³ In the three-in-one intensified
39
40 process, reaction conversion, crystal yield, agglomerate yield, the purity levels in the
41
42 solution and solid phase, granular flowability, friability, strength, tabletability and
43
44 dissolution rate will be fully investigated. Finally, to pave the way for scaling up the
45
46
47
48
49
50
51
52
53
54
55
56
57
58
59
60

1
2
3
4 three-in-one intensified process for dimethyl fumarate in the future, a 10 L-sized
5
6
7 vessel will be used to prove the feasibility as well.
8
9

10 11 12 **2. MATERIALS AND METHODS** 13

14 15 **2.1. Chemicals and Solvents** 16

17
18 Dimethyl fumarate (C₆H₈O₄, 99% purity, MW = 144.13, mp = 102-105°C, Lot:
19
20 10177580) and fumaric acid (C₄H₄O₄, 99% purity, MW = 116.07, mp = 299°C, Lot:
21
22 10175189) were purchased from Alfa Aesar (Heysham, England). Monomethyl
23
24 fumarate (C₅H₆O₄, 97% purity, MW = 130.1, mp = 144-145°C, Lot: MKBW0455V)
25
26 was purchased from Aldrich (St. Louis, MO, USA). Phenol red (C₁₉H₁₄O₅S, MW =
27
28 354.38, mp > 300°C, Lot: N07A006) was purchased from Alfa Aesar (Ward Hill, MA,
29
30 USA). Sodium hydroxide (NaOH, 97% assay, MW = 40.00, mp = 318°C, Lot:
31
32 KX-2842), dimethyl sulfate (C₂H₆O₄S, 99% purity, MW = 126.13, bp = 188°C, Lot:
33
34 KW-3436C) and sulfuric acid (H₂SO₄, 97% assay, MW = 98.08, bp = 337°C, ρ = 1.84
35
36 g/cm³, Lot: 4A267) were received from Showa Chemical Co. Ltd. (Tokyo, Japan).
37
38 Methanol (CH₃OH, 99.9% assay, MW = 32.04, bp = 64.7°C, Lot: 14050368) was
39
40 purchased from Tedia Company Inc. (Fairfield, OH, USA). Toluene (C₆H₅CH₃, ACS
41
42 grade 99.5% purity, MW = 92.14, bp = 111°C, Lot: ETA140403) and ethanol (C₂H₆O,
43
44 99.5% purity, MW = 46.7, bp = 78°C, Lot: 262611) were obtained from Echo
45
46
47
48
49
50
51
52
53
54
55
56
57
58
59
60

1
2
3
4 Chemical (Miaoli, Taiwan). Dimethyl sulfoxide-d₆ (DMSO-d₆, (CD₃)₂SO, 99 atom
5
6 % D, MW = 84.17, Lot: A0372803) was purchased from Acros Organics (New Jersey,
7
8 NJ, USA). Acetonitrile (CH₃CN, HPLC grade, MW = 41.05, bp = 82°C, Lot:
9
10 0000142848), and monopotassium phosphate (KH₂PO₄, MW = 136.086, mp =
11
12 252.6°C, Lot: 0000154227) were purchased from Avantor Performance Materials, Inc.
13
14 (Center Valley, PA, USA). Phosphoric acid (H₃PO₄, 85% assay, MW = 97.994, bp
15
16 = 158°C, Lot: K3422573 504) was purchased from Merck KGaA (Darmstadt,
17
18 Geremany). Reversible osmosis (RO) water was clarified by a water purification
19
20 system (model Milli-RO Plus) bought from Millipore (Billerica, MA, USA).
21
22
23
24
25
26
27
28
29
30
31
32

33 **2.2. Three-in-One Intensified Process of Reaction, Crystallization and** 34 35 **Spherical Agglomeration of Dimethyl Fumarate** 36

37
38 Three-in-one intensified process was carried out in a 0.5 L-sized jacketed glass
39
40 stirred tank with an inner diameter of 7.5 cm, equipped with four equally spaced
41
42 vertical baffles with a width of 9 mm, a four-bladed 45° turbine impeller with a
43
44 diameter of 3.5 cm¹⁹ and the clearance of the impeller from the vessel bottom was
45
46 lowered to 1.5 cm due to the small solution volume, a water jacket and a total reflux
47
48 condenser to prevent product loss.
49
50
51
52
53
54

55
56 For esterification, 8.357 g (0.072 mol) of fumaric acid were introduced to a 0.5
57
58
59
60

1
2
3
4 L-sized jacketed glass stirred tank. The tank was then heated to the maximum
5
6 allowable reaction temperature of 65°C (Supporting Information). 100 mL of
7
8 preheated methanol at the corresponding reaction temperature were then rapidly
9
10 added. The agitator was set to at 600 rpm. Once fumaric acid was dissolved, to
11
12 initiate the reaction, 0.96 mL of sulfuric acid (molar ratio of fumaric acid to sulfuric
13
14 acid = 4:1) was fed into the stirred tank by a glass pipette in one portion below the
15
16 liquid surface and near the tip of the impeller for good micro-mixing. The total
17
18 reaction time was 3 h. The percent reaction conversion is defined as: the number of
19
20 moles of reacted fumaric acid that divided by the initial 0.072 mol of fumaric acid fed
21
22 to the stirred tank multiplied by 100%.
23
24
25
26
27
28
29
30
31

32
33 For crystallization, the stirring speed was kept at 600 rpm. The clearance of
34
35 the impeller from the vessel bottom was adjusted from 1.5 to 3 cm because of (1) the
36
37 increase in solution volume, and (2) the consistency with our last study.¹⁹ 300 mL of
38
39 cold water as an anti-solvent at either 5°C or 25°C were rapidly fed into the same
40
41 stirred tank near the tip of the agitator through a funnel within about 1.5 min. The
42
43 stirred tank was cooled to either 5°C or 25°C with the cooling rate of 0.86°C/min for 3
44
45 h. Percent crystal yield is defined as: the actual yield of crystals, in grams, divided
46
47 by the theoretical yield of crystals, in grams, based on the reaction conversion
48
49 multiplied by 100%, assuming that the solubility of dimethyl fumarate is negligible in
50
51
52
53
54
55
56
57
58
59
60

1
2
3
4 the 1:3 (v/v) methanol-water mother liquor from 5° to 25°C.
5
6

7 For spherical agglomeration, 6 mL of toluene¹⁹ as a bridging liquid in a glass
8
9 pipette were added rapidly to the dimethyl fumarate suspension below the liquid
10
11 surface, near the tip of the impeller, which was stirred for 2 h. After the 2-h
12
13 maturation time, the spherical agglomerates were filtered out, and oven dried at 40°C
14
15 until no change in weight. The percent agglomerate yield is calculated by dividing
16
17 the actual yield of agglomerates, in grams, by the theoretical yield of agglomerates, in
18
19 grams, based on the reaction conversion multiplied by 100%, assuming that the
20
21 solubility of dimethyl fumarate is negligible in the 1:3 (v/v) methanol-water mother
22
23 liquor from 5° to 25°C.
24
25
26
27
28
29
30
31
32
33
34
35

36 **2.3. Disconnection of Spherical Agglomeration of Dimethyl Fumarate**

37

38 SA of dimethyl fumarate was done separately and disconnected from the train
39
40 of reaction and crystallization process. However, the operation conditions for the
41
42 remaining two steps of reaction and crystallization of dimethyl fumarate were
43
44 unchanged. Filtration would now be carried out after 3 h of crystallization process,
45
46 and oven drying of wet cakes was performed at 40°C until no change in weight. For
47
48 the disconnected SA, about 7 to 8 g of dried dimethyl fumarate crystals were first
49
50 introduced to a 0.5 L-sized jacketed glass stirred tank, and 400 mL of water at the
51
52
53
54
55
56
57
58
59
60

1
2
3
4 corresponding crystallization temperature of 5° or 25°C were then added. The
5
6
7 agitator was set to 600 rpm to make the slurry suspend. 6 mL of toluene as a
8
9
10 bridging liquid in a glass pipette were added rapidly to the dimethyl fumarate
11
12
13 suspension below the liquid surface near the tip of the impeller for good micromixing,
14
15
16 which was stirred for 2 h. After the 2-h maturation time, the round granules were
17
18
19 filtered out and oven dried at 40°C until no change in weight.
20
21
22
23

24 **2.4. Large Scale for Three-in-One Intensified Process of Dimethyl Fumarate**

25
26

27 Three-in-one intensified process was carried out in a 10 L-sized jacketed glass
28
29
30 stirred tank with an inner diameter of 20.4 cm, equipped with four equally spaced
31
32
33 vertical baffles with a width of 2.8 cm, a four-bladed 45° turbine impeller with a
34
35
36 diameter of 7 cm having a clearance from the vessel bottom of 3 cm, and a total reflux
37
38
39 condenser to prevent product loss. For esterification, 167.14 g (1.44 mol) of fumaric
40
41
42 acid were introduced to a 10 L-sized tank. 2 L of preheated methanol at 65°C were
43
44
45 then rapidly added. The agitator was set to at 350 rpm based on the Zwietering
46
47
48 equation.¹⁹ Once fumaric acid was dissolved, to initiate the reaction, 19.2 mL of
49
50
51 sulfuric acid (molar ratio of fumaric acid to sulfuric acid = 4:1) was fed into the
52
53
54 stirred tank by a dropping funnel in one portion below the liquid surface and near the
55
56
57 tip of the impeller for good micro-mixing. The total reaction time was 3 h. For
58
59
60

1
2
3
4 crystallization, the stirring speed was kept at 350 rpm. The clearance of the impeller
5
6
7 from the vessel bottom was adjusted from 3 to 7 cm because of the increase in
8
9
10 solution volume.¹⁹ 6 L of cold water as an anti-solvent at either 5°C or 25°C were
11
12
13 rapidly fed into the same stirred tank near the tip of the agitator through a dropping
14
15
16 funnel within about 5 min. For spherical agglomeration, 120 mL of toluene in a
17
18
19 dropping funnel were added rapidly to the dimethyl fumarate suspension below the
20
21
22 liquid surface, near the tip of the impeller, which was then stirred for 2 h. After the
23
24
25 2-h maturation time, the spherical agglomerates were filtered out, and oven dried at
26
27
28 40°C until no change in weight.

32 33 **2.5. Analytical Methods for Reaction Kinetics Study**

34
35
36 The kinetics of esterification was studied by the method of initial rates for a set
37
38
39 of initial fumaric acid concentrations of 0.36, 0.54 and 0.72 M in 100 mL solution at a
40
41
42 constant temperature of 45°, 55° and 65°C (Supporting Information). The maximum
43
44
45 allowable reaction temperature was determined by the reaction kinetics (Supporting
46
47
48 Information) to avoid the runaway situation.

52 53 **2.5.1. Gravimetric Analysis**

54
55
56 1-mL samples were withdrawn periodically through a glass pipette and titrated
57
58
59
60

1
2
3
4 against 1 M of methanolic NaOH solution with the addition of a drop of phenol red
5
6
7 pH indicator solution to determine the reactant concentration of fumaric acid.³⁴ An
8
9
10 excess amount of NaOH would be added to ensure all unreacted fumaric acid was
11
12
13 converted to white sodium fumarate precipitate as indicated by the color change of
14
15
16 phenol red from yellow to bright pink in the mother liquor. Each sample was
17
18
19 centrifuged at 6000 rpm for 10 min and then decanted. To avoid the undesired
20
21
22 dimethyl fumarate crystals mixed with sodium fumarate in the wet centrifuged cake,
23
24
25 the cake was rinsed with copious amount of methanol, centrifuged again with a speed
26
27
28 of 6000 rpm for 10 min and decanted. All sodium fumarate wet cakes were vacuum
29
30
31 dried at 40°C until no change in weight. The weight of each wet cake at different
32
33
34 time point was used to estimate the conversion of fumaric acid as a function of time.
35
36
37
38

39 **2.5.2. Nuclear Magnetic Resonance (NMR) Analysis**

40
41 To verify the validity of the simple and on-site gravimetric analysis, 1-mL
42
43
44 samples were also withdrawn periodically from the 0.5 L-sized jacketed glass stirred
45
46
47 tank to determine the reactant concentration of fumaric acid in one of the trials with
48
49
50 an initial fumaric acid concentration of 0.72 M at 45°C. All withdrawn samples
51
52
53 were immediately dropped into an ice bath to extinguish esterification. All samples
54
55
56 were vacuum dried at 0°C for 1 h to evaporate off methanol, water, monomethyl
57
58
59
60

1
2
3
4 sulfate (MMS), dimethyl sulfate (DMS), and sulfuric acid. Dimethyl fumarate solids
5
6
7 mixed with unreacted fumaric acid were obtained and their sublimation was
8
9
10 minimized at such a low temperature. About 50 mg of lyophilized reaction mixture
11
12
13 were dissolved in an adequate amount of deuterated dimethyl sulfoxide (DMSO-d₆).
14
15
16 About 0.8 mL of the DMSO-d₆ sample solution was added into an NMR tube having a
17
18
19 5-mm O.D. and 178 mm in length for solution ¹H NMR quantitative analysis. The
20
21
22 concentration of each sample was calculated by comparing the integral peak area for
23
24
25 the -COO-CH₃ ester proton chemical shift at 3.74 ppm with the one from a 0.25 M
26
27
28 dimethyl fumarate standard solution prepared by dissolving the purchased dimethyl
29
30
31 fumarate with a purity of 99% in DMSO-d₆ through the Top Spin 3.5 software from
32
33
34 Bruker (Billerica, Massachusetts, USA).
35
36
37

38 **2.5.3. Solubility Test**

39
40
41 About 10 mg of solid samples of dimethyl fumarate were weighed in a 20 mL
42
43
44 scintillation vial. Solvent or solution drops were titrated carefully by a micropipet
45
46
47 into the vial with intermittent shaking until all solids were just dissolved. The
48
49
50 solubility value of solids in the solvent or solution at a given temperature was
51
52
53 calculated as the weight of solids divided by the total volume of solvent or solution
54
55
56 added to the vial. Solubility values of solids in a solvent or solution at four different
57
58
59
60

1
2
3
4 temperatures of 15°, 25°, 40° and 60°C were determined in a water bath. Although
5
6 this particular gravimetric method for solubility determination³⁵ appeared to have an
7
8 inherent inaccuracy of about ±10%, its advantages were its robustness, simplicity,
9
10 without the need of performing any calibration and the concern of solvate formation.
11
12
13
14
15
16
17

18 **2.6. Sieve Analysis Method**

20
21 To determine the size distribution of dimethyl fumarate crystals/agglomerates,
22
23 a series of metal sieve plates from the largest to the finest aperture were utilized in the
24
25 order of 2000, 1410, 1000, 710, 500, 355, 250, 180, 125 and 90 μm (Kuang Yang,
26
27 Taiwan). About 1 to 5 g of dried samples were fed onto the 2000 μm sieve plate
28
29 directly and vibration was then generated by holding the 2000 μm-sized sieve plate
30
31 with one hand and tapping the sieve plate sideways with a spatula by another until no
32
33 more powders (or agglomerates) on the 2000 μm-sized sieve plate passed through by
34
35 eye. The same procedure was carried out repeatedly on the following smaller-size
36
37 opening sieve plates until the finest powder passed through the 90-μm sized sieve
38
39 plate and collected by the bottom receiver. The weight of the remaining particles on
40
41 each sieve plate was recorded and then divided by the total powder weight to obtain
42
43 the corresponding mass percent on sieve plotted as a histogram and cumulative mass
44
45 percent larger. With this method, there was no need to worry about factors which
46
47
48
49
50
51
52
53
54
55
56
57
58
59
60

1
2
3
4 may affect the end results like loading and time.
5
6
7
8

9 10 **2.7. Mechanical Properties of Spherical Agglomerates**

11 12 **2.7.1. Density of Spherical Agglomerates**

13
14
15 40 to 80 round granules of dimethyl fumarate in the size range of 710 to
16
17
18 1000 μm were selected and weighted. The diameter of round granules was 710 and
19
20
21 1000 μm on the average assuming each agglomerate was a sphere. The density was
22
23
24 calculated by dividing the mass of all agglomerates with the total spherical volumes of
25
26
27 agglomerates.
28
29
30
31
32

33 **2.7.2. Porosity of Spherical Agglomerates**

34
35
36 Porosity is a measurement of the void spaces in a material and its value is
37
38
39 between 0 and 1. If the void spaces are filled with air, the porosity, ϕ , can be defined
40
41
42 as:
43

$$44 \quad \phi = 1 - \frac{\rho_{bulk}}{\rho_{particle}}$$

45
46
47
48
49
50
51
52
53
54
55
56
57
58
59
60
(1)

where the bulk density (g/cm^3), ρ_{bulk} = mass of agglomerates divided by the volume of
agglomerates, the particle density (g/cm^3), $\rho_{particle}$ = true density of solids ($\rho_{dimethyl}$
fumarate = 1.12 g/cm^3).³⁶

2.7.3. Carr's Index

A portion of 710 to 1000 μm round granules was poured into a 5 mL graduated cylinder. The flowability of agglomerates were quantified by the Carr's index, CI, defined as:¹⁹

$$\text{CI} = \frac{\rho_t - \rho_p}{\rho_t} \times 100\% \quad (2)$$

where the poured density (g/cm^3), ρ_p = mass of agglomerates divided by the undisturbed volume in a 5 mL graduated cylinder after filling, and the tapped density (g/cm^3), ρ_t = mass of agglomerates divided by the disturbed volume after tapping until no change in the volume was seen. The number of times for tapping was about 100.

2.7.4. Friability

0.5 g of the 710 to 1000 μm round granules was placed in a 50 mL scintillation vial with a 35-mm O.D. and 58 mm in length which was subjected to a rotating speed of 50 rpm on a ball-milling machine (MUBM-236-RTD, Shin Kwan Machinery, Taipei) for 30 min.³⁷ The weight of 710- to 1000- μm sized round granules before and after this friability test was measured. Friability of round granules was determined by using the formula.³⁸

$$\text{Friability}(\%) = \frac{W_0 - W}{W_0} \times 100\% \quad (3)$$

where W_0 = initial weight of the round granules placed on the 710- μm sized sieve, W = weight of the round granules did not pass through the 710- μm sized sieve after rotation.

2.7.5. Particle Strength

The fracture forces of 10 to 30 granules from the same size cut of 710 to 1000 μm were determined together by compression under a punch with a water reservoir.¹⁹ Water titration would continue until all round granules were fractured due to the increasing weight of the water reservoir. The force applied was the total weight of water and the water reservoir, and the average fracture force exerted on each round granule was the total force applied divided by the number of granules.

2.7.6. Tableability

Tableability is the ability to make a tablet of adequate mechanical strength by powder compaction. 200 mg of 710- to 1000- μm sized round dimethyl fumarate granules were charged into the 13 mm die set of the FT-IR pellet press (Specac Inc., Woodstock, GA, USA) with about 8 tons of compaction force to produce a tablet.

2.8. Dissolution Test

A dissolution test station (SR6, Hanson Research Corporation, Chatsworth, California) Type II (paddle method) at a rotational speed of 100 rpm was used for *in vitro* testing of the dissolution behavior of dimethyl fumarate crystals. Dissolution was carried out on 120 mg of the size range of 710-1000 μm dimethyl fumarate agglomerates. RO water of pH 6.8 with potassium phosphate buffer was used as the dissolution medium. The volume and temperature of the dissolution medium were 500 mL and $37.0 \pm 0.2^\circ\text{C}$, respectively. 1-mL samples were withdrawn at the time points of 0, 1, 2.5, 5, 6.5, 8, 10, 12.5, 15, 20, 30, 40, 60, 90 and 120 min by a plastic syringe near the stirring paddle. Each sample was filtered by a 0.22 μm PVDF membrane (PALL Corporation, PN), diluted 40 times in a 20 mL scintillation vial with RO water, and then assayed for the absorbance of dimethyl fumarate by UV-vis spectrophotometer at $\lambda = 210 \text{ nm}$. The concentration of dimethyl fumarate at each time point was converted from the absorbance value to the corresponding concentration by a linear calibration: Absorbance (a.u.) = $116.4 \times$ Concentration of dimethyl fumarate (mg/mL), according to Beer's law established from five standard dimethyl fumarate solutions, each with a known concentration of dimethyl fumarate.

2.9. Analytical Instrumentations

2.9.1. Thermocouple

The solution temperature in the 0.5 L baffled glass reactor was recorded by a K-type thermocouple and a temperature logger (TM-947SD, Lutron Electronic, Taipei, Taiwan)

2.9.2. Nuclear Magnetic Resonance Spectroscopy (NMR)

^1H NMR was used for carbon-hydrogen framework, concentration and impurity determination. All of the ^1H NMR spectra were performed at 298 K using Bruker Avance III HD spectrometer at 600 MHz proton frequency with 5 mm BBFO probe in Z-gradient.

2.9.3. Gas Chromatography–Mass Spectroscopy (GC-MS)

The GC–MS analyses for samples were performed on a Thermo Scientific Trace 1300 Gas Chromatograph instrument coupled with a Thermo Scientific ISQ Single Quadrupole mass-selective detector and a Thermo Scientific autosampler TriPlus RSH injector. A Rxi-5MS capillary column with a dimension of 30 m \times 0.25 mm I.D. \times 0.25 μm film thickness was used for the chromatographic separation. The initial oven temperature was 40°C, and then increased to 160°C at a rate of 10°C/min.

1
2
3
4 The injection size was 1 μL , which was prepared by dissolving about 2 mg of sample
5
6 in 1 mL of methanol. Helium was used as the carrier gas with a constant flow rate of
7
8 1 mL/min. The injector and MS source temperatures are set at 180° and 250°C,
9
10 respectively. The electron impact (EI) mode at 70 eV was utilized for sample
11
12 ionization. The GC-MS spectra for DMS and internal standards were obtained
13
14 through the injection of the stock solutions and scanning in the range of m/z 29–300.
15
16
17
18
19
20
21 The GC-MS chromatograms are recorded with selected ion monitoring (SIM) mode.
22
23
24
25
26

27 **2.9.4. High Performance Liquid Chromatography (HPLC)**

28
29
30 HPLC measurement of samples was performed using a Shimadzu LC-20AT
31
32 HPLC with SIL-20A autosampler and SPD-20A UV/vis spectrophotometric detector.
33
34
35 Sample solution was prepared by about 10 mg of sample dissolving in 20 mL of
36
37 methanol. 5 μL of sample drop was injected onto a YMC-Pack reverse phase
38
39 ODS-AQ 250 mm \times 4.6 mm I.D. \times 5 μm particle size \times 12 nm pore size column with a
40
41 mobile phase of 0.01M $\text{H}_3\text{PO}_4/\text{ACN}$ (80/20 v/v) pumped at 0.8 mL/min. Sample
42
43 was detected by its native UV absorbance at $\lambda = 220$ nm.
44
45
46
47
48
49
50
51
52

53 **2.9.5. Gas Chromatography (GC)**

54
55
56 Gas chromatographic analysis was carried out by using a China
57
58
59
60

1
2
3
4 Chromatography 2000 fitted with a flame ionization detector. Nitrogen was used as
5
6 the carrier gas and was set at 15 mL/min. The separation was performed with a 10%
7
8 Carbowax 20M phase, matrix 80/100 Chromosorb W-HP column, 3 m × 1/8 in O.D. ×
9
10 2.1 mm I.D. (SUPELCO metal packed GC column). The oven temperature and the
11
12 injector temperature were set at 190°C and 200°C, respectively. The detector
13
14 temperature were set at 190°C and 200°C, respectively. The detector
15
16 temperature was held at 220°C. About 15 mg of sample was dissolved in 1 mL of
17
18 ethanol. The injection volume for a sample was 1 µL.
19
20
21
22
23
24
25
26

27 **2.8.6. Fourier Transform Infrared (FT-IR) Spectroscopy**

28
29
30 Infrared spectroscopy provided information about the kinds of functional
31
32 groups in the molecule. FT-IR spectroscopy was conducted on Perkin Elmer
33
34 Spectrum One (Norwalk, CT, USA). 1 mg of each sample was ground gently with
35
36 99 mg of KBr powders, then a manual press was used to form the pellet. The pellet
37
38 was scanned 8 times with a resolution of 2 cm⁻¹ in the region of 4000 to 400 cm⁻¹.
39
40
41
42
43
44
45
46

47 **2.8.7. Differential Scanning Calorimetry (DSC)**

48
49
50 DSC analysis was mainly used to identify the enthalpy of fusion, solid-liquid
51
52 (melting) temperature, and solid-solid transition temperature. Thermal analytical
53
54 data of samples in perforated aluminum sample pans were collected on a Perkin Elmer
55
56
57
58
59
60

1
2
3
4 DSC-7 calorimeter (Perkin Elmer Instruments LLC, Shelton, CT, USA) with a
5
6
7 temperature scanning rate of 10°C/min from 30° to 150°C under a constant nitrogen of
8
9
10 99.990% purge.

11 12 13 14 15 **2.8.8. Powder X-Ray Diffraction (PXRD)**

16
17
18 The PXRD diffractogram detected by Bruker D8 Advanced (Germany) could
19
20
21 provide information about crystal structure identification and crystallinity. The
22
23
24 source of PXRD was Cu K α ($\lambda = 1.542 \text{ \AA}$) and the diffractometer was operated at 40
25
26
27 kV and 40 mA. The scanning rate was set at 0.05° 2 θ /sec ranging from 5° to 35°,
28
29
30 and the experiment was operated under room temperature.

31 32 33 34 35 **2.8.9. Single Crystal X-ray Diffraction (SXD)**

36
37
38 SXD provided detailed information about the internal lattice of crystalline
39
40
41 substances, including unit cell dimensions, bond-lengths, bond-angles, and details of
42
43
44 site-ordering. SXD data of dimethyl fumarate samples were obtained from the
45
46
47 literature.³⁰ The view of crystal structure from SXD was drawn by Diamond 3.1
48
49
50 computer software (Crystal Impact GbR, Brandenburg Germany).

51 52 53 54 55 **2.8.10. Optical Microscopy (OM)**

1
2
3
4 To observe the actual size of dimethyl fumarate primary crystals, the dried
5
6 dimethyl fumarate powders harvested from antisolvent and cooling crystallization step
7
8 were dispersed in mineral oil, birefringence and crystal habits were observed by
9
10 Olympus BX-51 (Tokyo, Japan) equipped with a digital camera (Hong Kong, China)
11
12 Moticom 2000. These images were transformed by Moticom Images Plus (version 2.0)
13
14 into digital pictures and analyzed by Measure Tool (version 4.10, copyright by
15
16 Jie-chuang international Co., Ltd.) The other optical microscope (Olympus SZII,
17
18 Tokyo, Japan) with a charge couple device (CCD) camera (SONY, model:
19
20 SSCDC50A, Tokyo, Japan) was used to characterize the morphology of dimethyl
21
22 fumarate granules.
23
24
25
26
27
28
29
30
31
32
33
34
35

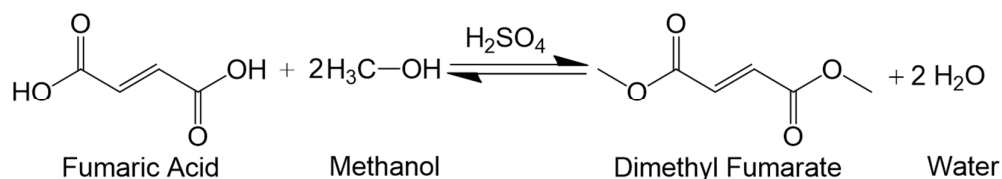
36 **2.8.11. Ultraviolet Visible (UV/Vis) Spectrophotometer**

37
38 UV/Vis spectrophotometer was used to identify organic compounds and
39
40 measure concentrations of solutions. The clear solution was assayed for dimethyl
41
42 fumarate based on the characteristic UV absorbance peak at 210 nm by an UV/vis
43
44 spectrophotometer (Lambda 25, Perkin-Elmer, Norwalk, CT, USA.).
45
46
47
48
49
50
51
52

53 **3. RESULTS AND DISCUSSION**

54 **3.1. Reaction**

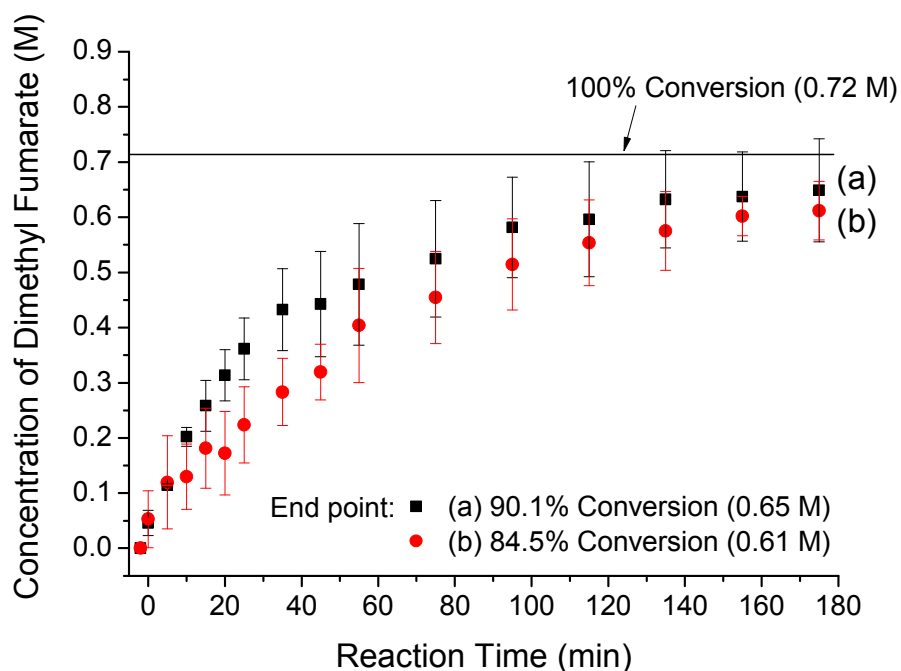
1
2
3
4 Dimethyl fumarate was prepared by sulfuric acid-catalyzed esterification of
5
6 fumaric acid with methanol (Scheme 1). This was a classical homogeneous
7
8 liquid-phase reaction.³¹ Guzowski *et al.* had reported of using the different molar
9
10 ratios of fumaric acid to sulfuric acid of 4:1, 20:1 and 100:1 and achieved the same
11
12 conversion to dimethyl fumarate when reacted for 3, 8 and 18 h, respectively.²⁹ In
13
14 this study, the molar ratio of fumaric acid to sulfuric acid of 4:1 was chosen for
15
16 achieving a reasonable reaction time length. The initial concentration of sulfuric
17
18 acid catalyst was fixed at 0.73 mol% (2.18 wt%) in the methanolic reaction medium.
19
20 However, the larger amount of sulfuric acid used in esterification could raise the level
21
22 of side products such as monomethyl sulfate MMS and DMS.²⁹ Due to the
23
24 genotoxic nature of DMS, its maximum daily intake level should not exceed 1.5 μg
25
26 per person per day,³⁹ and the risk of creating MMS and DMS must be carefully
27
28 evaluated.
29
30
31
32
33
34
35
36
37
38
39
40
41



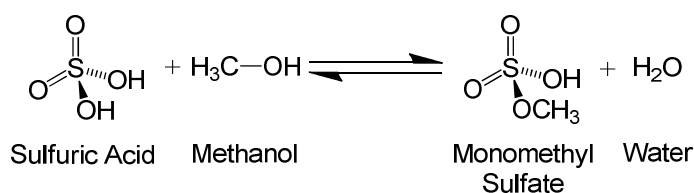
Scheme 1. Esterification of fumaric acid and methanol.

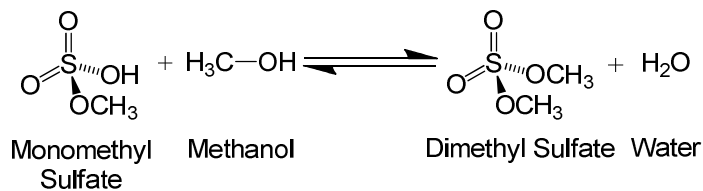
The ¹H NMR spectra in Figures S1(a) to S1(p) revealed the kinetics of esterification of fumaric acid with methanol (Scheme 1) in different time samples. The chemical shifts for alkene protons of fumaric acid and dimethyl fumarate slightly

1
2
3
4 moved from 6.61 ppm (Peak (I)) to 6.77 ppm (Peak (1)) during the progress of
5
6
7 esterification. The integral peak area of the resonance for the $-\text{COO}-\text{CH}_3$ ester
8
9
10 protons at 3.71 ppm (Peak (2)) did grow over time. The total reaction time of 3 h
11
12 was sufficient to reach a $\sim 85\%$ conversion (Figure 1). Because of the low
13
14 concentration of sulfuric acid used, esterification of sulfuric acid was suppressed
15
16
17
18 (Scheme 2).³⁹
19
20
21
22
23



46
47
48 **Figure 1.** Kinetic studies of esterification of fumaric acid with an initial concentration
49 of 0.72 M based on 100 mL of methanol at 45°C by (a) gravimetric analysis, and (b)
50 ¹H NMR analysis (based on Figures S1(a) to S2(p)).
51

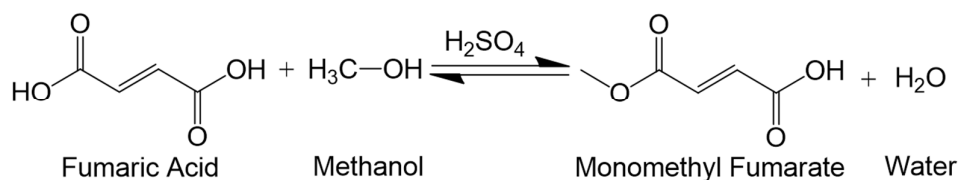




10
11
12
13
14
15
16
17
18
19
20
21
22
23
24
25
26
27
28
29
30
31
32
33
34
35
36
37
38
39
40
41
42
43
44
45
46
47
48
49
50
51
52
53
54
55
56
57
58
59
60

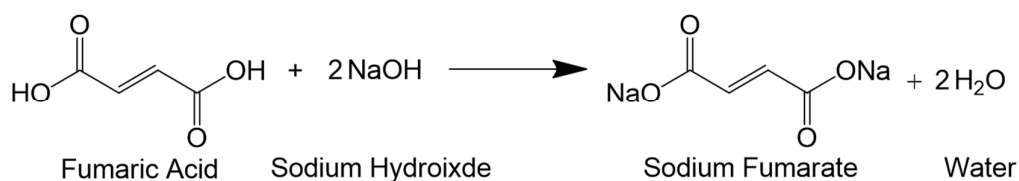
Scheme 2. Esterification of sulfuric acid and methanol.

Noticeably, the chemical shift of hydroxyl $-OH$ protons for fumaric acid showed a broad singlet with a large downfield shift at 13.06 ppm (Peak (II)) because of the high initial concentration of $-OH$ protons and increased hydrogen bonding in DMSO- d_6 (Figure S1). As the esterification proceeded, fumaric acid was being consumed and its concentration was lowered. The $-OH$ proton signal then moved to a higher chemical shift to around 4.78 ppm (Peak (7)) due to the diminishing solvent effect. In general, the chemical shift for $-OH$ proton is strongly dependent on concentration, temperature, and solvent.⁴⁰ The peak of reaction intermediate, monomethyl fumarate (MMF) (Scheme 3), at chemical shift of methyl $-CH_3$ proton around 3.72 ppm (Peak (8)) was detected in the beginning of esterification. However, it was gradually decreased over time, and finally disappeared towards the end of reaction (Figure S1 Insets). For the other chemical shifts at 2.50 ppm (Peak (3)), 3.16 ppm (5)) and 3.38 ppm (Peak (4)), they were from the protons of DMSO- d_6 , methanol, and water in “neat” DMSO- d_6 , respectively.



Scheme 3. Formation of monomethyl fumarate.

All concentrations of fumaric acid were obtained indirectly by gravimetric analysis of sodium fumarate based on Scheme 4. The simple and on-site gravimetric analysis was adequate for the rapid estimation of the reaction rates under our current situations where in-house gas chromatography-mass spectroscopy (GC-MS) and high performance liquid chromatography (HPLC) were unavailable. The validity of our gravimetric analysis was verified by comparing the concentrations of fumaric acids determined from the kinetic experiment having an initial concentration of 0.72 M in 100 mL of methanol at 45°C with the concentrations of dimethyl fumarate of the same time points directly obtained from ^1H NMR (Figures S1 and 1).



Scheme 4. Formation of sodium fumarate in gravimetric analysis.

The two concentration versus time curves of dimethyl fumarate from the gravimetric analysis and ^1H NMR in Figure 1 displayed the same rising trend and reached a conversion of ~ 90% in 3 h. However, the concentrations determined from

¹H NMR were always lower than the ones from the gravimetric method because small amount of dimethyl fumarate was sublimed upon vacuum drying during the NMR sample preparation step.

The maximum allowable operating temperature was determined by the kinetics of esterification. Esterification with three different initial fumaric acid concentrations of 0.36, 0.54 and 0.72 M in 100 mL solution at 45°C were conducted. The concentration profiles of fumaric acid and dimethyl fumarate were shown in Figure S2. For the determination of activation energy, experiments for a series of reaction temperatures of 45°, 55° and 65°C in 100 mL solution at the same initial concentration of 0.72 M were performed as illustrated in Figure S3. According to the experimental results, esterification of fumaric acid with methanol was a first-order reaction and the rate expression was (Supporting Information, Equation (S6)):

$$-r_{\text{fumaric acid}} = kC_{\text{fumaric acid}}^1 = Ae^{-\frac{E_a}{RT}}C_{\text{fumaric acid}} \quad (4)$$

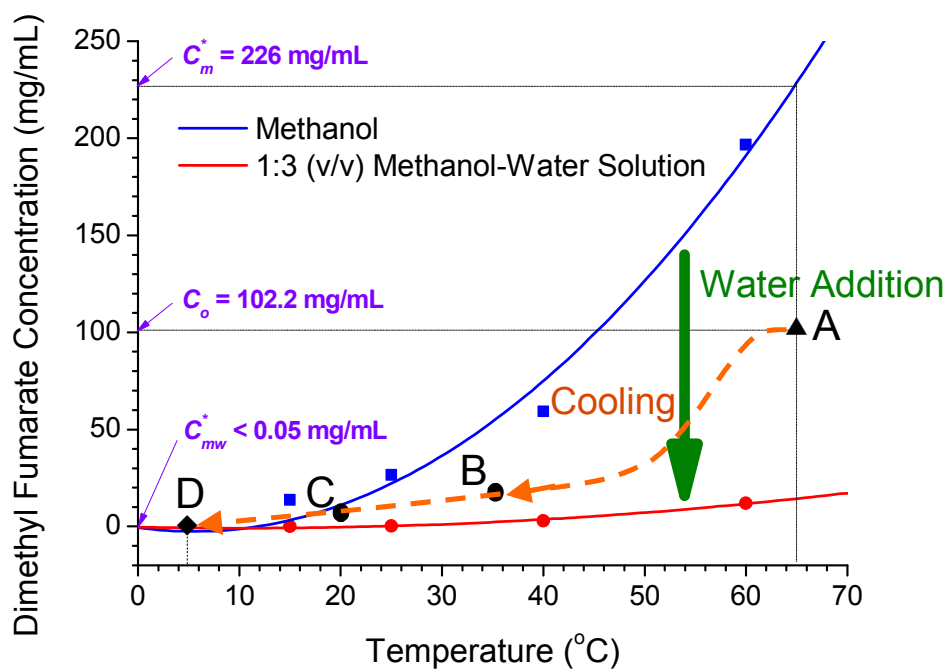
where $-r_{\text{fumaric acid}}$ = the rate of disappearance of fumaric acid ($\text{mol}\cdot\text{L}^{-1}\cdot\text{min}^{-1}$); k = intrinsic rate constant (min^{-1}); $C_{\text{fumaric acid}}$ = the concentration of fumaric acid ($\text{mol}\cdot\text{L}^{-1}$); $R = 8.314 \text{ J}\cdot\text{mol}^{-1}\cdot\text{K}^{-1}$; T = temperature (K); E_a = the activation energy = 4.05×10^4 ($\text{J}\cdot\text{mol}^{-1}$) and A = frequency factor = 1.33×10^5 (min^{-1}). Since our E_a value was very close to the one of 44,400 ($\text{J}\cdot\text{mol}^{-1}$) for the esterification of acetic acid with methanol

1
2
3
4 in the presence of hydrogen iodide, our gravimetric method was reliable. The rate
5
6
7 equation could be used for the design of a large-scale reactor, the prediction of the
8
9
10 equilibrium composition, reaction end-point, conversion, and the safety assessment.
11
12 Figure S4 predicted that the reaction ended at 180, 120 and 90 min for the
13
14 esterification of dimethyl fumarate at 45°, 55° and 65°C, respectively, in an adiabatic
15
16 system. To ensure all reactions were truly complete, the reaction time for all
17
18 temperatures was fixed at 180 min. According to Figure S4, in a 65°C operation
19
20 with an initial fumaric acid concentration of 0.72 M, the reactor temperature could be
21
22 raised above the boiling point of methanol of 64.9°C by 8.6°C if the heat generated
23
24 from esterification could not be removed effectively. Since our stirred tank was
25
26 water jacketed, equipped with a stirrer and containing only a small volume of 100 mL
27
28 methanol, it was safe to run the reaction to as high as 65°C due to sufficient heat
29
30 transfer and heat removal.
31
32
33
34
35
36
37
38
39
40
41
42
43
44

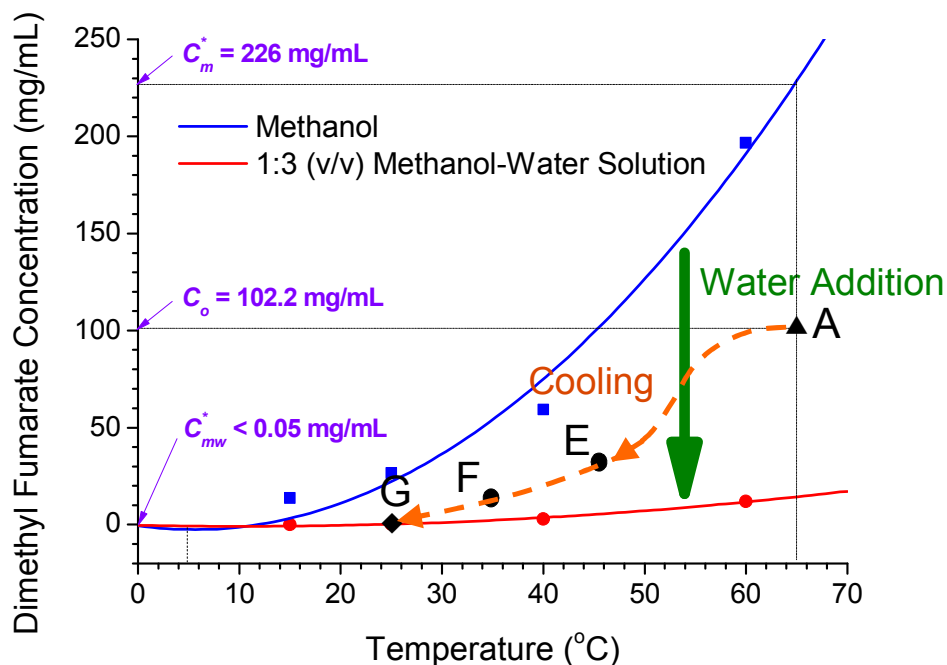
45 3.2. Crystallization

46
47 After 3 h of esterification, the reaction was extinguished upon the addition of
48
49 cold water and crystallization began to take place. The two different crystallization
50
51 pathways from (1) 65° to 5°C (Crystallization I), and (2) 65° to 25°C (Crystallization
52
53 II), and solubility curves of dimethyl fumarate in (1) methanol, and (2) 1:3 (v/v)
54
55
56
57
58
59
60

1
2
3
4 methanol-water solution, were displayed together in Figure 2. After esterification in
5
6
7 100 mL methanol at 65°C, the solution represented by Point A with an initial dimethyl
8
9
10 fumarate concentration, C_0 , of 102.2 mg/mL was located way below the solubility
11
12 value of dimethyl fumarate in methanol, C_m^* , of 226 mg/mL (Figure 2(a)). The
13
14 initial supersaturation ratio, $S_0 = C_0/C_m^* = 102.2 \text{ mg/mL} / 226 \text{ mg/mL} = 0.45 < 1$,
15
16 means that the solution was unsaturated and stable. Upon the addition of 300 mL
17
18
19 cold water at 5°C, the solvent makeup and temperature were instantly changed. The
20
21
22 solubility value of dimethyl fumarate in 1:3 (v/v) methanol-water solution became
23
24
25 C_{mw}^* of $< 0.05 \text{ mg/mL}$ at 5°C which was much less than C_m^* , of 226 mg/mL at 65°C,
26
27
28 so that S_0 had then become $S_0' = C_0/C_{mw}^* = 102.2 \text{ mg/mL} / 0.05 \text{ mg/mL} = 2044 \gg 1$.
29
30
31
32 The solution became highly supersaturated and labile. Suddenly, Point A was found
33
34
35 to be located above the solubility curve of dimethyl fumarate in 1:3 (v/v)
36
37
38 methanol-water solution. If the mixture was rapidly cooled from Point A to 5°C,
39
40
41 spontaneous Crystallization I would occur and plunge the system to Point B near
42
43
44 35.4°C (Figure 3(a)). The system followed the processing pathway of $A \rightarrow B \rightarrow C$
45
46
47 $\rightarrow D$. The dimethyl fumarate concentration in the solution would keep decreasing
48
49
50 until an equilibrium dimethyl fumarate concentration at 5°C of $\ll 0.05 \text{ mg/mL}$ at
51
52
53 Point D was reached (Figure 3(a)).
54
55
56
57
58
59
60



(a)



(b)

Figure 2. Solubility curves of dimethyl fumarate versus temperature in methanol, and 1:3 (v/v) methanol-water solution. Schematic diagrams of crystallization routes: (a)

Crystallization I, and (b) Crystallization II.

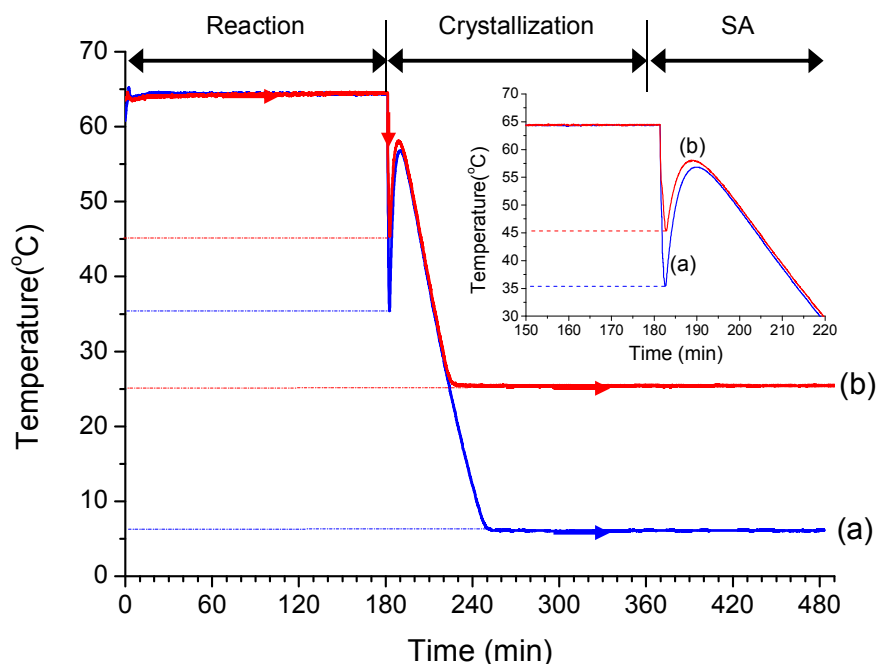


Figure 3. Temperature–history curves of 0.5 L three-in-one intensified process of (a) 65° to 5°C in crystallization step, and (b) 65° to 25°C in crystallization step.

A similar situation also occurred for Crystallization II in 100 mL methanol at 65°C. The solution represented by Point A with an initial dimethyl fumarate concentration, C_0 , of 102.2 mg/mL was located just below the solubility value of dimethyl fumarate in methanol, C_m^* , of 226 mg/mL (Figure 2(b)). After the cold water addition at 25°C, the solubility of 1:3 (v/v) methanol-water solution was lowered to C_{mw}^* , of < 0.05 mg/mL. $S_0 = C_0/C_m^*$ had then become $S_0' = C_0/C_{mw}^* = 102.2 \text{ mg/mL} / 0.05 \text{ mg/mL} = 2044 \gg 1$. The solution suddenly turned supersaturated and unstable. Point A was then located way above the solubility

1
2
3
4 curve of dimethyl fumarate in the 1:3 (v/v) methanol-water solution. Spontaneous
5
6
7 Crystallization II driven by the large S_0' followed the processing pathway of A → E →
8
9
10 F → G with a valley near 45.4°C (Figure 3(b)). The dimethyl fumarate
11
12
13 concentration in the solution would keep decreasing until an equilibrium dimethyl
14
15
16 fumarate concentration of $\ll 0.05$ mg/mL at Point G of 5°C was reached (Figure
17
18
19 2(b)). Since the S_0' of Crystallization I was higher than the one of Crystallization II,
20
21
22 and the slope of the processing pathway from A → B → C was steeper than the one
23
24
25 from A → E → F, a larger number of nuclei would be generated and resulted in a
26
27
28 smaller particle size distribution for Crystallization I.

29
30 The optical micrographs in Figures 4(a) and 4(b) showed that dimethyl
31
32
33 fumarate solids dispersed in mineral oil were platy and highly crystalline due to
34
35
36 birefringence. It was evidence that crystals produced from Crystallization I were 50
37
38
39 μm which were smaller than the 100 μm sized primary crystals from Crystallization II.
40
41
42 The percent crystal yields were 75.5% and 69.7% for Crystallization I and II,
43
44
45 respectively. However, aggregates are usually formed when primary small particles
46
47
48 tend to be held together more by cohesive and electrostatic forces in a dried form.³²
49
50
51 This was in agreement with the dry sieve analysis in Figure 4. The size distribution
52
53
54 of about 55.6 wt% for aggregates of > 90 μm and > 125 μm from the batch of
55
56
57 Crystallization I was indeed higher than 29.1 wt% for aggregates of the same size cuts
58
59
60

from the batch of Crystallization II.

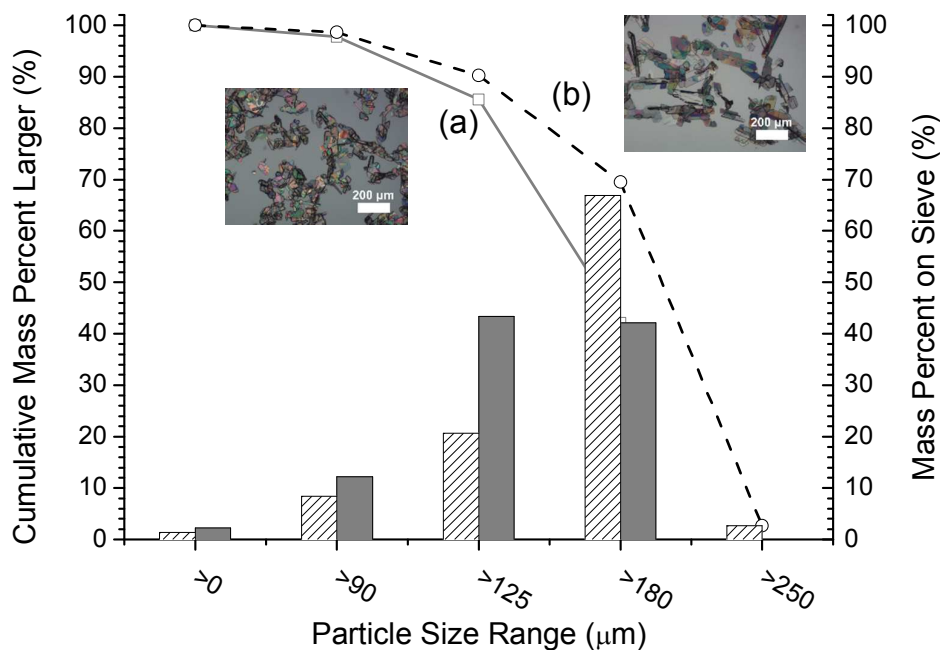


Figure 4. The particle size distribution, cumulative mass percent larger and optical micrographs of dimethyl fumarate crystals produced from (a) 0.5 L-Crystallization I (solid/gray), and (b) 0.5 L-Crystallization II (dash/shaded).

3.3. Spherical Agglomeration

Toluene was chosen as the bridging liquid for the SA method because of the relatively good solubility of dimethyl fumarate in toluene near 20.4 ± 1.7 mg/mL at 5°C and 49.2 ± 1.8 mg/mL at 25°C . The SA process was the interplay of events of particle-to-particle adhesion due to the presence of bridging liquid, particle-to-particle collision, particle-to-impeller collision, particle-to-baffle collision, and the balance

1
2
3
4 between cohesion and disruption.^{19,41-43} Therefore, the weight % of a given size cut
5
6
7 of agglomerates in Figure 5 could be viewed as the actual yield of that particular size
8
9
10 cut of agglomerates in the batch. That particular agglomerate size was governed by
11
12 the growth events of the agglomerate in the stirred tank, which was related to a family
13
14 of specific traveling pathways. Those pathways were directed by the streamlines and
15
16 the Stokes number for collisions. The number of possible and successful pathways
17
18 from a certain hydrodynamics pattern could be sensitive to the initial particle size
19
20 when all other operating parameters such as bridging liquid volume to solid ratio
21
22 (BSR), baffle configuration, stirring rate and maturation time were held constant.¹⁹
23
24
25 In addition, solid loading also influences the final agglomerate size. The
26
27 agglomerate size decreases with the increase in solid loading.⁴⁴ Therefore, the
28
29 amount of dimethyl fumarate crystals produced from chemical synthesis in a given
30
31 liquid volume must be maintained at a certain ratio.
32
33
34
35
36
37
38
39
40
41
42
43
44
45
46
47
48
49
50
51
52
53
54
55
56
57
58
59
60

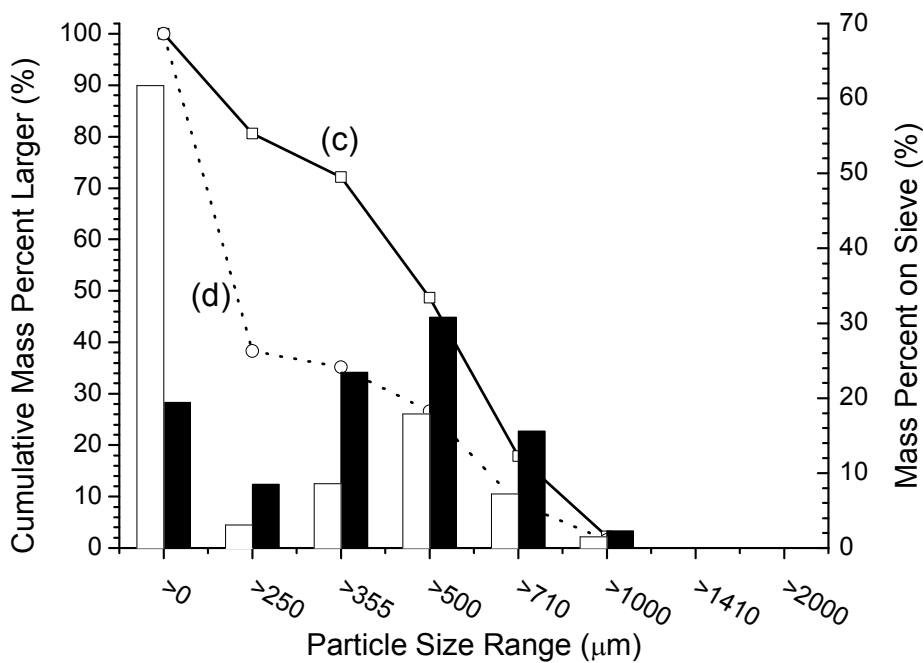
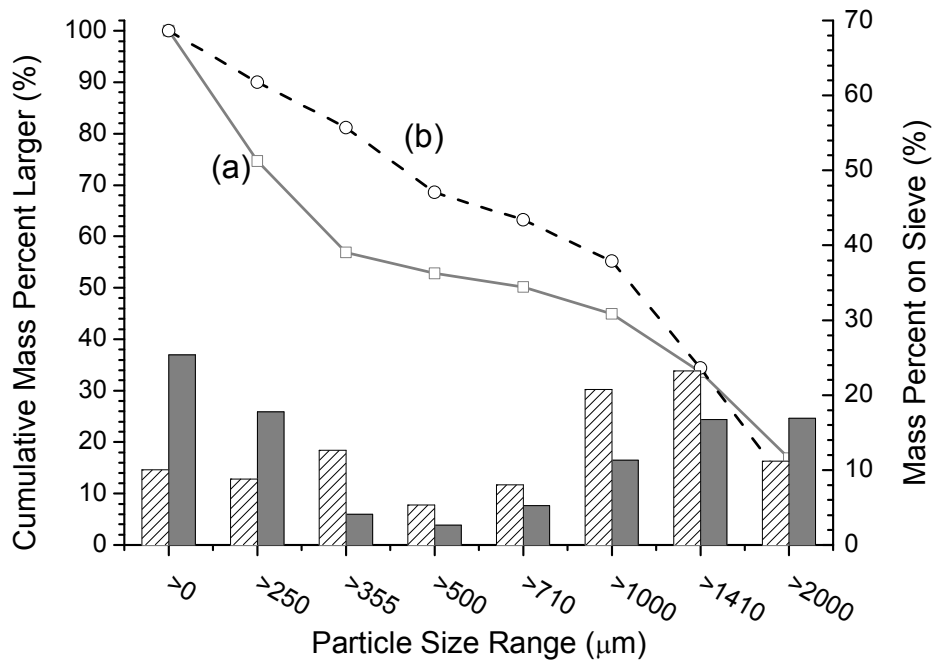


Figure 5. The particle size distribution and cumulative mass percent larger of dimethyl fumarate agglomerates produced from (a) 0.5 L-Three-in-one I (solid/gray), (b) 0.5 L-Three-in-one II (dash/shaded), (c) 0.5 L-SA I (solid/black) and 0.5 L-SA II (dotted/white).

1
2
3
4
5 The primary crystals from Crystallization I produced at 5°C were smaller than
6
7
8 the ones from Crystallization II generated at 25°C. Although the surface area per
9
10
11 volume of the small primary crystals from Crystallization I was much larger than the
12
13
14 one of the large primary crystals from Crystallization II, the binding ability of the
15
16
17 bridging liquid (toluene) was increased in from SA at 5°C to SA at 25°C because of
18
19
20 the higher solubility of dimethyl fumarate in toluene. Therefore, we speculate that
21
22
23 the round granules produced from the primary crystals of Crystallization I produced at
24
25
26 5°C would be smaller than the ones made from the primary crystals of Crystallization
27
28
29 II produced at 25°C. It was evidenced in Figure 5 that SA based on Crystallization
30
31
32 I (Three-in-one I) gave a large number of agglomerates of > 2000 μm whereas SA
33
34
35 based on Crystallization II (Three-in-one II) shifted to the majority of larger
36
37
38 agglomerates of > 710 μm, > 1000 μm and > 1410 μm. Therefore, the general trend
39
40
41 for the PSD was transferable from crystallization to spherical agglomeration given
42
43
44 with all operating parameters were constant. The optical images in Figures 6(a) and
45
46
47 6(b) show that the particles above 500 μm and 355 μm, from Three-in-one I and II,
48
49
50 respectively, were truly round granules. On the other hand, the disconnected SA
51
52
53 processes based on Crystallization I and II, namely, SA I and II, respectively, would
54
55
56 give smaller agglomerate sizes of less than 1000 μm. Particles from SA I and II
57
58
59 from 250 to 710 μm were true granules as displayed in Figures 6(c) and 6(d). Our
60

1
2
3
4 granular size range of 250-2000 μm generated from Three-in-one I and II, and SA I
5
6
7 and II, was comparable with the size ranges of: 400-760 μm from Peña and Nagy,¹⁶
8
9
10 300-800 μm from Tahara *et al.*,¹⁷ 368-600 μm from Jitkar *et al.*,²¹ 100-3000 μm from
11
12 Li *et al.*,²⁰ 355-1000 μm from Lin *et al.*,¹⁹ 80-500 μm from Nocent *et al.*,⁴⁵ and
13
14
15 280-1250 μm from Katta and Rasmuson.⁴⁶
16
17
18
19
20
21
22
23
24
25
26
27
28
29
30
31
32
33
34
35
36
37
38
39
40
41
42
43
44
45
46
47
48
49
50
51
52
53
54
55
56
57
58
59
60

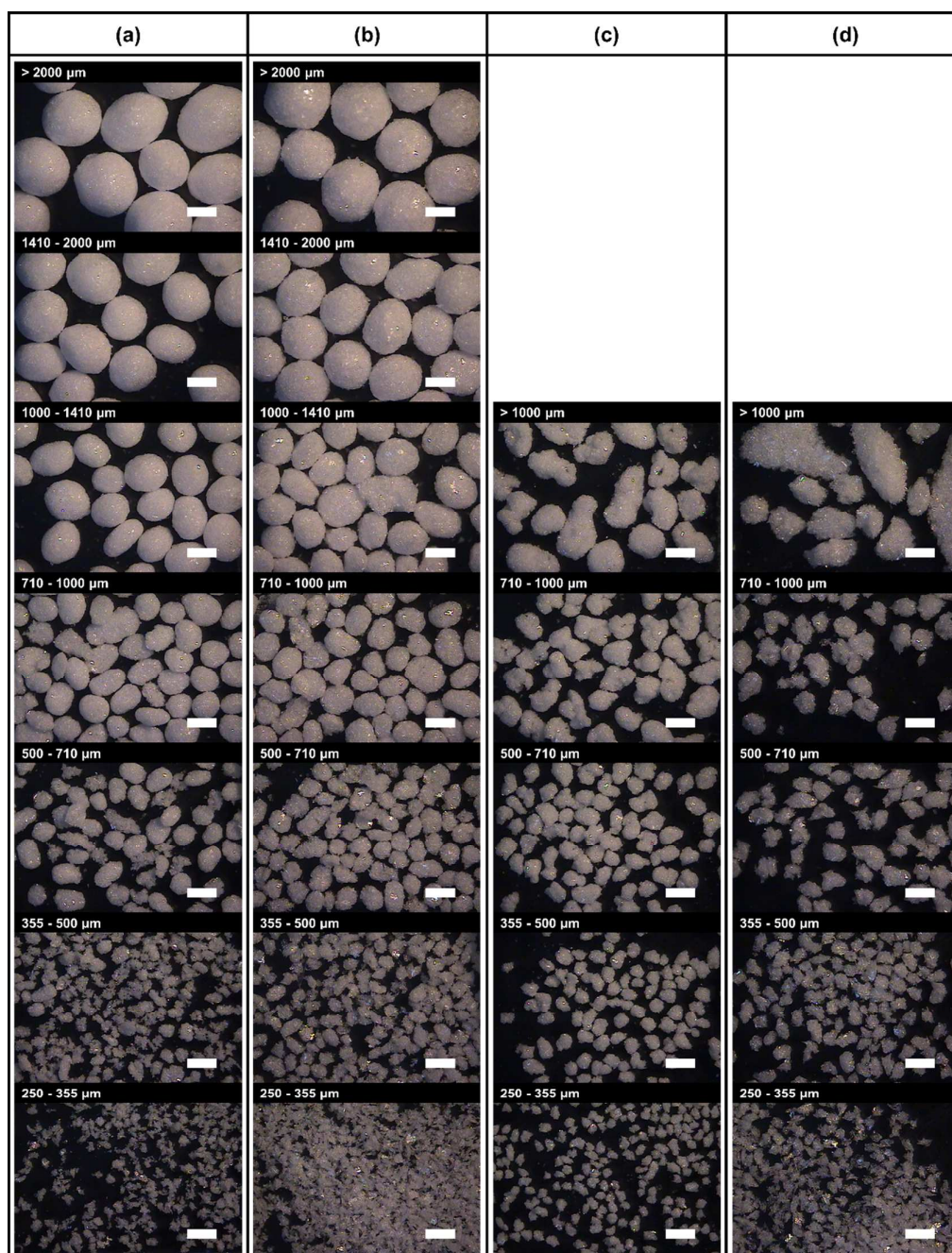


Figure 6. OM images of dimethyl fumarate agglomerates from (a) Three-in-one I, (b) Three-in-one II, (c) SA I and (d) SA II. (scale bare = 1000 μm)

Only the 710-1000 μm sized round granules were large enough for mechanical properties characterization (Table 1). Agglomerates from Three-in-one I and II and SA I had a similar low Carr's Index of less than 15% exhibiting an excellent

1
2
3
4 free-flowing property, which is beneficial to downstream processing in general such
5
6
7 as compression and tableting. However, the granules from Three-in-one II having
8
9
10 the lowest friability of $10.4\pm 3.19\%$ and the highest fracture force of 0.095 ± 0.007 N
11
12
13 per granule displayed a much better mechanical strength than the granules from other
14
15
16 processes (Table 1). The round granules from Three-in-one I and II had a higher
17
18
19 density of 0.84 ± 0.06 and 0.83 ± 0.04 g/cm³ than the ones of 0.79 ± 0.06 and 0.78 ± 0.04
20
21
22 g/cm³, from SA I and II, respectively. The percent agglomerate yields were 72.7,
23
24
25 68.8, 60.6 and 65.7% for round granules from Three-in-one I and II, and SA I and II,
26
27
28 respectively. The mechanical properties of the round granules produced from the
29
30
31 disconnected SA were weaker than the ones from the three-in-one intensified process.
32
33
34 In the disconnected SA, the oven dried dimethyl fumarate was used as the starting
35
36
37 material which was difficult to be wetted and dispersed. Most of the aggregates had
38
39
40 already been held together by cohesive and electrostatic forces in a dried form. On
41
42
43 the other hand, in the three-in-one intensified process, the primary crystals used in SA
44
45
46 were nucleated and grown directly from crystallization without drying. They were
47
48
49 well dispersed and wetted uniformly with toluene binder in the subsequent SA step.
50
51
52 Since toluene could dissolve dimethyl fumarate, a relatively strong and round
53
54
55 granules were produced due to the homogeneous formation of solid bridges among
56
57
58 primary crystals by dissolution-re-precipitation.
59
60

Table 1. Physical and mechanical properties of 710 to 1000 μm sized agglomerates.

	Density (g/cm^3)	Porosity	Carr's Index (%)	Friability (%)	Fracture Force (N)
Three-in-one I	0.84 \pm 0.06	0.25 \pm 0.05	8.83 \pm 0.23	15.04 \pm 1.54	0.048 \pm 0.003
Three-in-one II	0.83 \pm 0.04	0.26 \pm 0.03	13.64 \pm 3.10	10.36 \pm 3.19	0.095 \pm 0.007
SA I	0.79 \pm 0.06	0.29 \pm 0.05	10.26 \pm 1.67	27.04 \pm 2.54	0.026 \pm 0.003
SA II	0.78 \pm 0.04	0.30 \pm 0.03	16.67 \pm 3.03	29.86 \pm 3.15	0.011 \pm 0.002

3.4. Dissolution Performance

Dissolution rates of the size range of 710-1000 μm dimethyl fumarate round granules prepared from Three-in-one I and II, SA I and II, and bulk dimethyl fumarate crystals harvested from Crystallization I and II were further compared in Figure 7. The dissolution rate of crystals grown from Crystallization II was much faster than the one of crystals from Crystallization I even though the crystals from Crystallization I were smaller. This was probably due to the aggregation of the small crystals from Crystallization I by cohesive and electrostatic forces in a dried form. Polar solvent like water was unable to wet the interstitial surfaces of dimethyl fumarate aggregates with air and fail to disperse the primary crystals effectively.

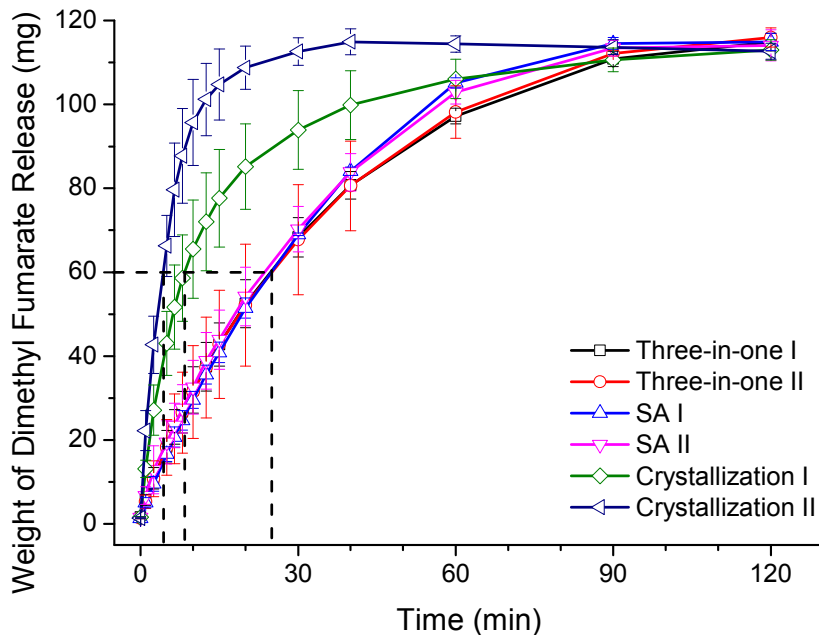


Figure 7. Dissolution profiles of 710- to 1000- μm sized dimethyl fumarate agglomerates grown from 0.5 L-Three-in-one I, 0.5 L-Three-in-one II, 0.5 L-SA I, 0.5 L-SA II, 0.5 L-Crystallization I and 0.5 L-Crystallization II, respectively.

On the other hand, it took about the same time of 25 min to dissolve 50 wt% of all round granules from Three-in-one I and II, and SA I and II. Apparently all dissolution profiles followed the rate law, dC/dt , at which a solid substance dissolved in its own solution was proportional to the difference between the concentration of the saturated solution, C_s , and the concentration of that solution, C_b , as:

$$\frac{dC}{dt} = \frac{DS}{hV}(C_s - C_b)$$

(5)

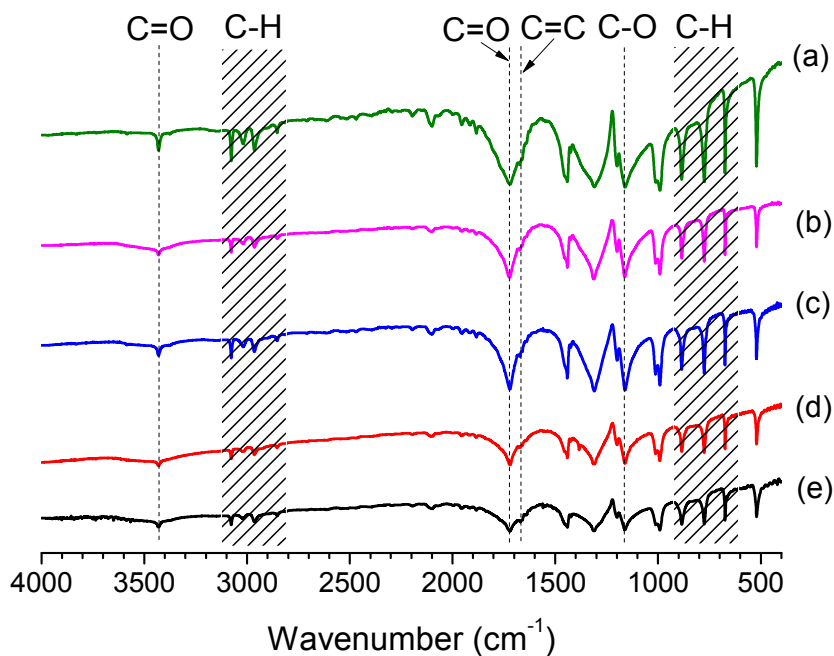
according to the film theory, where D was the diffusion coefficient of the solute; S was the specific surface area; h was the thickness of the diffusion layer; and V was the

1
2
3
4 volume of the dissolution medium.³² Given that all parameters were constant, the
5
6
7 dissolution performance was only proportional to the exterior surface area, S , of the
8
9
10 granules regardless of the processing history and the PSD of the primary crystals.
11
12 As a result, SA could be used as a technique for fixing the unwanted properties of
13
14 primary crystals inherited from different methods. No polymorphic transformation
15
16 or hydration of dimethyl fumarate had occurred during dissolution.
17
18
19
20
21
22
23

24 3.5. Analysis and Characterization

25
26
27 HPLC chromatograms in Figure S5 showed that the impurity levels of fumaric
28
29 acid and MMF were below 0.1% for all dimethyl fumarate crystals and round
30
31 granules. The retention times for fumaric acid, MMF and dimethyl fumarate were
32
33 4.6, 7.5 and 18.9 min, respectively. Mass spectra (MS) of DMS and dimethyl
34
35 fumarate were shown in Figure S6 with $m/z = 66, 79$ and 95 chosen as the
36
37 characteristic signals for DMS quantitative analysis. GC-MS spectra in Figures S7
38
39 and S8 further indicated that retention times for purchased DMS and dimethyl
40
41 fumarate were 4.64 and 7.20 min, respectively. Figure S8 showed that no detectable
42
43 level of DMS was observed in all crystals and round granules. GC chromatograms
44
45 in Figure S9 indicated that retention times for dimethyl fumarate, toluene and ethanol
46
47 were 1.83, 0.69 and 0.52 min, respectively, and no residual toluene binder were
48
49
50
51
52
53
54
55
56
57
58
59
60

1
2
3
4 detected in all round dimethyl fumarate granules.
5
6
7
8
9
10



32 **Figure 8.** IR spectra of dimethyl fumarate (a) crystals from 0.5 L-Crystallization I, (b)
33 crystals from 0.5 L-Crystallization II, (c) round granules from 0.5 L-Three-in-one I, (d)
34 round granules from 0.5 L-Three-in-one II, and (e) commercial dimethyl fumarate
35 with a purity of 99%.
36
37
38
39
40
41
42
43
44
45
46
47
48
49
50
51
52
53
54
55
56
57
58
59
60

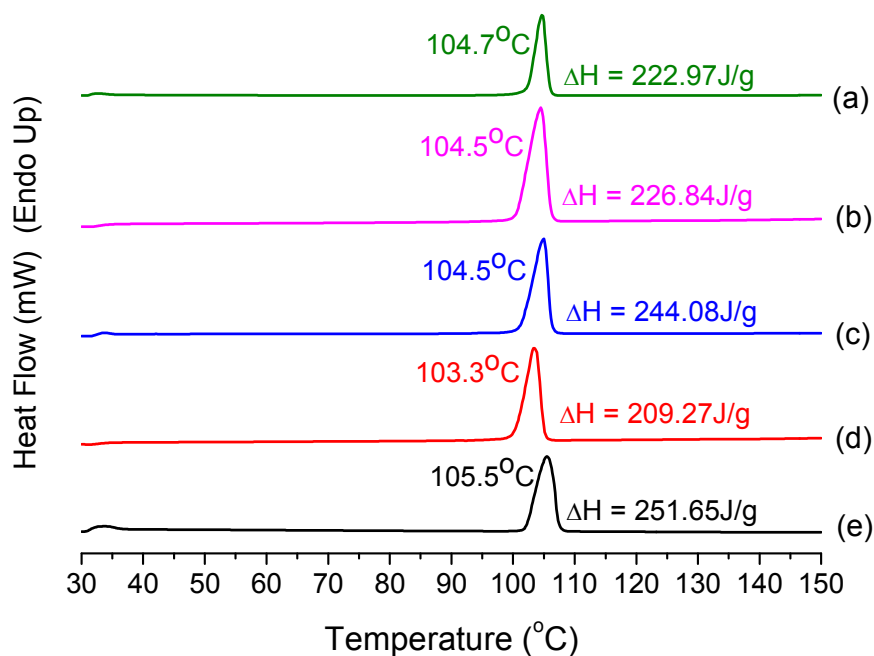


Figure 9. DSC scans of dimethyl fumarate (a) crystals from 0.5 L-Crystallization I, (b) crystals from 0.5 L-Crystallization II, (c) round granules from 0.5 L-Three-in-one I, (d) round granules from 0.5 L-Three-in-one II, and (e) commercial dimethyl fumarate with a purity of 99%.

The chemical purity and polymorphism of all dimethyl fumarate crystals obtained from Crystallization I and II and round granules from Three-in-one I and II were also thoroughly investigated by solid-state characterization methods such as IR, DSC and PXRD. Their results were compared with the commercially purchased dimethyl fumarate. No trace of impurity was observed in the IR spectra in Figure 8 as well. The IR spectra of all samples looked exactly identical with the assignments at 1672 cm^{-1} for the C=C stretching vibration, 1719 and 3430 cm^{-1} for the C=O stretching vibration, 1160 cm^{-1} for the C-O stretching vibration, and 670 - 890

1
2
3
4 cm^{-1} and $2850\text{-}3080\text{ cm}^{-1}$ for the C-H bending vibration. The DSC scans in Figure
5
6
7 9 illustrated that the melting points of all samples were close with one another near
8
9 103.3° to 105.5°C with the enthalpy of fusion from 209.27 to 251.65 J/g. All
10
11 samples appeared to be pure and isomorphous having a relatively high crystallinity
12
13 based on the high enthalpy of fusion. The PXRD patterns of all samples were
14
15 overlaid with the theoretical PXRD pattern from single-crystal X-ray diffraction data
16
17 for verifying their authenticity in Figure 10. All dimethyl fumarate samples had
18
19 identical crystal forms and exhibited the characteristic diffraction peaks at $2\theta = 11.0^\circ$,
20
21 17.6° , 22.1° , 24.1° and 27.5° corresponding to (001), (0 $\bar{1}$ 1), (002), ($\bar{1}$ 01), ($\bar{1}$ 11) planes.
22
23
24
25
26
27
28
29
30 The added values of free flowing and easy-to-pack properties to dimethyl fumarate in
31
32 addition to its original intrinsic slip planes in the crystal lattice should make direct
33
34 compaction of dimethyl fumarate into tablets feasible. Tablets as shown in Figures
35
36
37
38 11(a) and (b) were made by direct compaction of round granules generated from
39
40 Three-in-one I and II, respectively. Figure 11(c) suggested that plastic deformation
41
42 was contributed to the dislocation motion along the crystallographic ($\bar{1}$ 01) slip plane
43
44
45
46
47 of dimethyl fumarate.
48
49
50
51
52
53
54
55
56
57
58
59
60

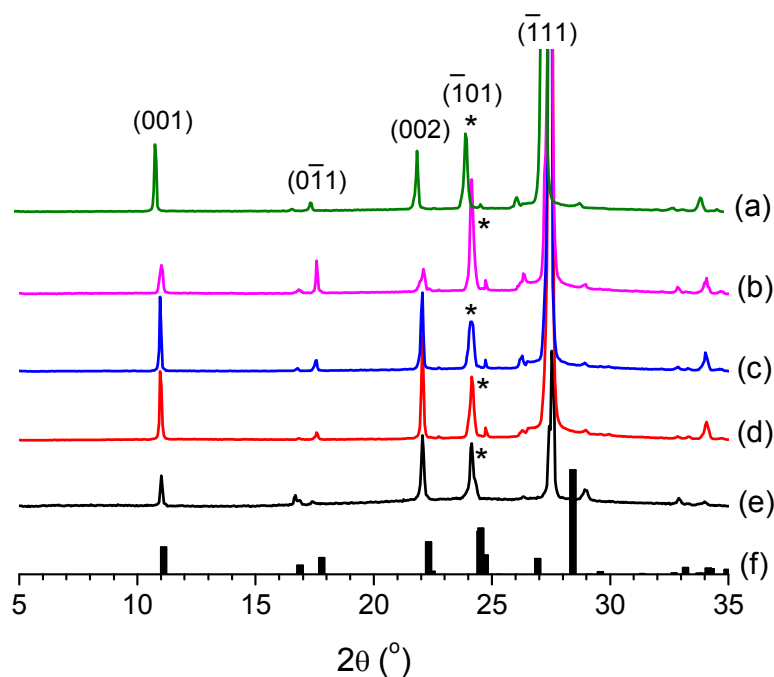
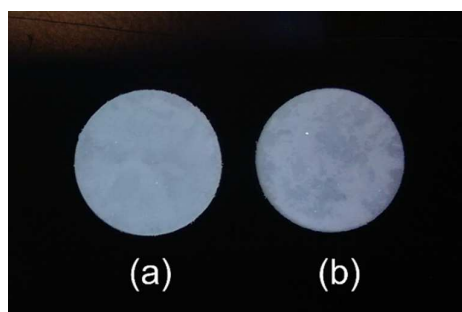


Figure 10. PXRD patterns of dimethyl fumarate (a) crystals from 0.5 L-Crystallization I, (b) crystals from 0.5 L-Crystallization II, (c) round granules from 0.5 L-Three-in-one I, (d) round granules from 0.5 L-Three-in-one II, (e) the commercial dimethyl fumarate with a purity of 99%, and (f) the theoretical PXRD of dimethyl fumarate (slip plane for dimethyl fumarate is designated by *).



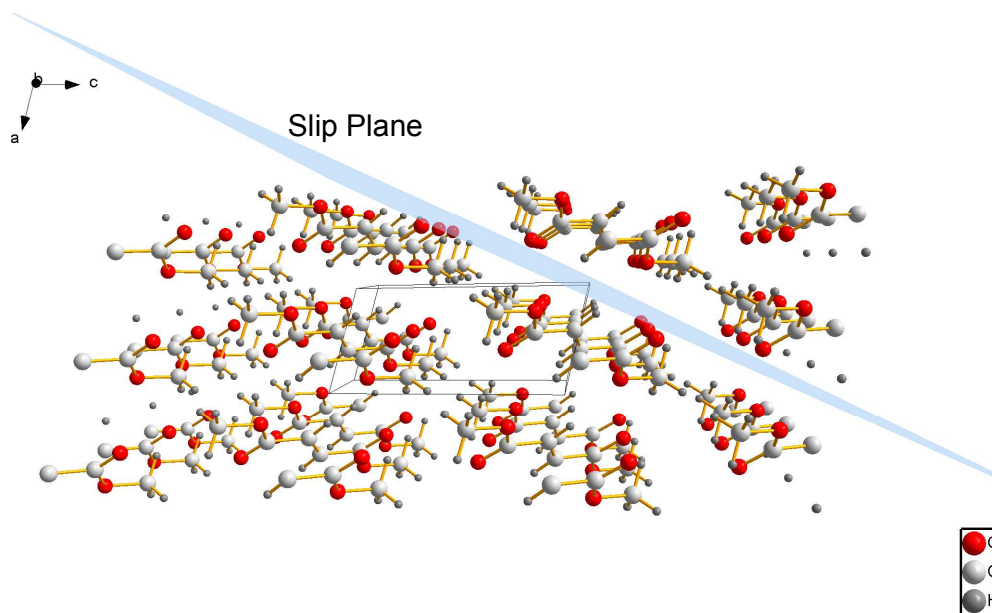


Figure 11. Digital image of dimethyl fumarate tablets from round granules made from (a) 0.5 L-Three-in-one I, (b) 0.5 L-Three-in-one II, and (c) view of the triclinic dimethyl fumarate unit cell having unit cell parameters of $a = 3.849\text{\AA}$, $b = 5.616\text{\AA}$, $c = 8.349\text{\AA}$, $\alpha = 100.71^\circ$, $\beta = 100.38^\circ$, $\gamma = 105.43^\circ$ with $(\bar{1}01)$ plane as the slip plane.

3.6. Effects of Tank Size

The same operating conditions used in a 0.5 L-sized tank were applied to a 10 L-sized tank. The time for reaction time, crystallization and spherical agglomeration were 3, 3 and 2 h, respectively. According to the HPLC analysis in Figures S5 (g) and (h), dimethyl fumarate with purity above 99.6% could still be obtained in the 10 L-sized scale after 3 h of reaction. The PSD of spherical agglomerates was shown in Figure 12, and true granules were again fallen in the range from 250 to 710 μm . Compared with the round granules from the 0.5 L-sized tank as illustrated in Figures 5(a) and 5(b), spherical agglomerates produced from 10 L-sized tank were shifted to

1
2
3
4 the smaller sizes. Since the formation of spherical agglomerates was through
5
6
7 particle-particle collision, particle-impeller collision and particle-baffle collision, the
8
9
10 number of collisions would be drastically reduced for traveling a longer distance in a
11
12
13 larger tank during the same 2 h of maturation time. Consequently, smaller granules
14
15 would result. Even so, the three-in-one intensified process of dimethyl fumarate
16
17 could still be applied to a large scale. The desired particle size range may be
18
19 obtained by prolonging the maturation time or by adding more bridging liquid in the
20
21
22
23
24
25
26
27
28
29
30
31
32
33
34
35
36
37
38
39
40
41
42
43
44
45
46
47
48
49
50
51
52
53
54
55
56
57
58
59
60

future.

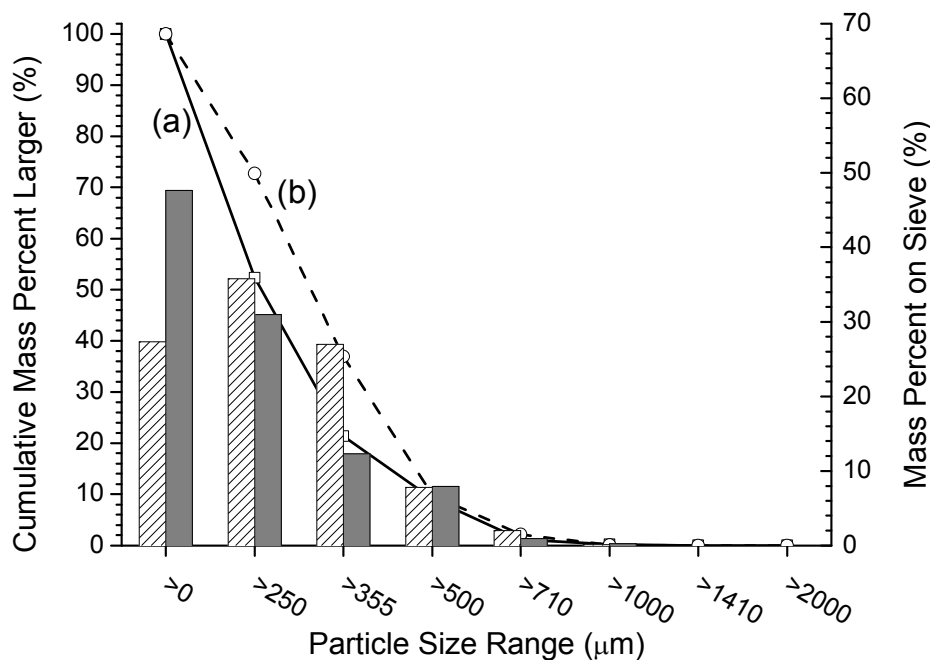


Figure 12. The particle size distribution and cumulative mass percent larger of dimethyl fumarate agglomerates produced from (a) 10 L-Three-in-one I (solid/gray), and (b) 10 L Three-in-one II (dash/shaded).

4. CONCLUSIONS

The bottom-up approach of synthesizing dimethyl fumarate, drowning it out as platy primary crystals, and then turning them into spherical agglomerates was successfully carried out in a common stirred tank. The low concentration of 2 wt% sulfuric acid used for esterification, and the appropriate reaction time length had completely prevented the presence of MMS and DMS in all the final products. The round granules generated from the three-in-one intensified process and the disconnected SA were pure in dimethyl fumarate, isomorphic, in the size range of 250 to 2000 μm , and free-flowing. Furthermore, the dissolution profiles were similar for granules which had the same size cut and independent from the processing history of the primary crystals. Therefore, SA coupled with the train of reaction and crystallization could add values to the API crystals. The free flowing and easy-to-pack properties to dimethyl fumarate in addition to its original intrinsic slip planes in the crystal lattice should make direct compaction of dimethyl fumarate into tablets feasible. The percent agglomerate yield was between 60 to 75% and the strength of the granules were relatively low. In the future work, granule strength would be optimized by increasing the maturation time, adding polymers as a bridging liquid, and decreasing the size of the primary particles.

ASSOCIATED CONTENT

Supporting Information

Kinetics experiments, Reaction enthalpy, Purity analysis by NMR, HPLC, GC-MS and GC, Equations S1 to S13, Tables S1 and S2, Figures S1 to S9. This information is available free of charge via the Internet at <http://pubs.acs.org>.

ACKNOWLEDGMENTS

This research is supported by grants from the Ministry of Science and Technology of Taiwan, R.O.C. (MOST 104-2221-E-008-070-MY3). We are greatly indebted to Ms. Hsiu-Luan Chen for the assistance with NMR of the Instrumentation Center at National Central University, Taiwan, R.O.C. We also thank Ms. Yun-Ming Li for the assistance with GC-MS of the Instrumentation Center at National Chiao Tung University, Taiwan, R.O.C, Ms. Jui-Mei Huang for DSC and all associated with of the Precision Instrument Center at National Central University, Taiwan, R.O.C., Ms. Pi-Lien Hung for the assistance with HPLC at Chunghwa Chemical Synthesis & Biotech Co., Ltd. and Professor Chieh-Ming Hsieh for the resistance with GC in the Department of Chemical and Materials Engineering at National Central University, Taiwan, R.O.C.

1
2
3
4
5
6
7
8
9
10
11
12
13
14
15
16
17
18
19
20
21
22
23
24
25
26
27
28
29
30
31
32
33
34
35
36
37
38
39
40
41
42
43
44
45
46
47
48
49
50
51
52
53
54
55
56
57
58
59
60

REFERENCES

- (1) Mollan, M. J.; Lodaya, M. Continuous Processing in Pharmaceutical Manufacturing. *Pharm. Manuf. Mag.* **2004**.
<http://www.pharmamanufacturing.com/assets/Media/MediaManager/ContinuousProcessinginPharmaManufacturing.doc>.
- (2) Wall Street Journal "Factory Shift: New Prescription for Drug Makers: Update the Plants." September 3, 2003.
- (3) Mollan, M. J., Jr.; Lodaya, M. Continuous Processing in Pharmaceutical Manufacturing. *Pharmaceutical Manufacturing Magazine* **2004**, October, 1–9.
- (4) Plumb, K. Continuous Processing in the Pharmaceutical Industry Changing the Mind Set. *Trans IChemE, Part A, Chem. Eng. Res. Des.* **2005**, 83(A6), 730-738.
- (5) Leane, M.; Pitt, K.; Reynolds, G.; The Manufacturing Classification System (MCS) Working Group. A Proposal for a Drug Product Manufacturing Classification System (MCS) for Oral Solid Dosage Forms. *Pharm. Dev. Technol.* **2015**, 20(1), 12-21.
- (6) Parikh, D. M. Continuous Granulation Technology Trends: Seeking a Smooth Path and Avoiding Dead Ends. *Contract Pharma* **2016**, June, 82-85.
- (7) Shanmugam, S. Granulation Techniques and Technologies: Recent Progresses. *BioImpacts* **2015**, 5(1), 55-63.

1
2
3
4
5 (8) Kleinebudde, P. Roll Compaction/Dry Granulation: Pharmaceutical Applications.
6
7

8 *Eur. J. Pharm. Biopharm.* **2004**, *58*(2), 317-326.
9

10 (9) Vervaet, C.; Remon, J. P. Continuous Granulation in the Pharmaceutical Industry.
11
12

13 *Chem. Eng. Sci.* **2005**, *60*(14), 3949-3957.
14
15

16 (10) Pasquali, I.; Bettini, R.; Giordano, F. Supercritical Fluid Technologies: An
17
18

19 Innovative Approach for Manipulating the Solid-State of Pharmaceuticals. *Adv.*
20

21 *Drug Deliv. Rev.* **2008**, *60*(3), 399-410.
22
23
24

25 (11) Mackaplow, M. B.; Rosen, L. A.; Michaels, J. N. Effect of Primary Particle
26
27

28 Size on Granule Growth and Endpoint Determination in High-Shear Wet Granulation.
29

30 *Powder Technol.* **2000**, *108*(1), 32-45.
31
32
33

34 (12) Bardin, M.; Knight, P. C.; Seville, J. P. K. On Control of Particle Size
35
36

37 Distribution in Granulation Using High-Shear Mixers. *Powder Technol.* **2004**,
38

39 *140*(3), 169-175.
40
41
42

43 (13) Park, J.-B.; Kang, C.-Y.; Kang, W.-S.; Choi, H.-G.; Han, H.-K.; Lee, B.-J. New
44
45

46 Investigation of Distribution Imaging and Content Uniformity of Very Low Dose
47

48 Drugs Using Hot-Melt Extrusion Method. *Int. J. Pharm.* **2013**, *458*(2), 245-253.
49
50

51 (14) Kawashima, Y.; Capes, C. E. Experimental Study of the Kinetics of Spherical
52
53

54 Agglomeration in a Stirred Tank. *Powder Technol.* **1974**, *10*(1-2), 85-92.
55
56

57 (15) Kawashima, Y.; Okumura, M.; Takenaka, H. Spherical Crystallization: Direct
58
59

1
2
3
4
5 Spherical Agglomeration of Salicylic Acid Crystals during Crystallization. *Science*
6
7
8 **1982**, 216(4550), 1127-1128.

9
10
11 (16) Peña, R.; Nagy, Z. K. Process Intensification through Continuous Spherical
12
13 Crystallization Using a Two-Stage Mixed Suspension Mixed Product Removal
14
15 (MSMPR) System. *Cryst. Growth Des.* **2015**, 15(9), 4225-4236

16
17
18 (17) Tahara, K.; O'Mahony, M.; Myerson, A. S. Continuous Spherical
19
20 Crystallization of Albuterol Sulfate with Solvent Recycle System. *Cryst. Growth*
21
22 *Des.*, **2015**, 15(10), 5149-5156.

23
24
25 (18) Lee, T.; Su, Y. C.; Hou, H. J.; Hsieh, H. Y. Spherical Crystallization for Lean
26
27 Solid-Dose Manufacturing (Part I). *Pharm. Technol.* **2010**, March, 72-75.

28
29
30 (19) Lin, P. Y.; Lee, H. L.; Chen, C. W.; Lee, T. Effects of Baffle Configuration and
31
32 Tank Size on Spherical Agglomerates of Dimethyl Fumarate in a Common Stirred
33
34 Tank. *Int. J. Pharm.* **2015**, 495(2), 886-894.

35
36
37 (20) Li, J.-S.; Wu, S.-W.; Lu, K.-T. Study on Preparation of Intensive and Spherical
38
39 High Bulk Density Nitroguanidine with Controllable Particle Size. *Propellants*
40
41 *Explos. Pyrotech.* **2016**, 41(2), 312-320.

42
43
44 (21) Jitkar, S.; Thipparabonia, R.; Chaven, R. B.; Shastri, N. R. Spherical
45
46 Agglomeration of Platy Crystals: Curious Case of Etodolac. *Cryst. Growth Des.*
47
48 **2016**, 16(7), 4034-4042.

1
2
3
4
5 (22) Lee, T.; Chen, J. W.; Lee, H. L.; Lin, T. Y.; Tsai, Y. C.; Cheng, S.-L.; Lee, S.-W.;
6
7
8 Hu, J.-C.; Chen, L.-T. Stabilization and Spheroidization of Ammonium Nitrate:
9
10 Co-Crystallization with Crown Ethers and Spherical Crystallization by Solvent
11
12 Screening. *Chem. Eng. J.* **2013**, *225*, 809-817.

13
14
15
16 (23) Quon, J. L.; Chadwick, K.; Wood, G. P. F.; Sheu, I.; Brettmann, B. K.; Myerson,
17
18 A. S.; Trout, B. L. Templated Nucleation of Acetaminophen on Spherical Excipient
19
20 Agglomerates. *Langmuir* **2013**, *29*(10), 3292-3300.

21
22
23
24
25 (24) Toddy, A. I.; Badruddoza, A. Z. M.; Zheng, L.; Alan Hatton, T.; Gunawan, R.;
26
27 Rajagopalan, R.; Khan, S. A. Spherical Crystallization of Glycine from
28
29 Monodisperse Microfluidic Emulsion. *Cryst. Growth Des.* **2012**, *12*(8), 3977-3982.

30
31
32
33
34 (25) Zhang, H.; Chen, Y.; Wang, J.; Gong, J. Investigation on the Spherical
35
36 Crystallization Process of Cefotaxime Sodium. *Ind. Eng. Chem. Res.* **2010**, *49*(3),
37
38 1402-1411.

39
40
41
42 (26) Luo, J.; Kong, F.; Ma, X. Role of Aspartic Acid in the Synthesis of Spherical
43
44 Vaterite by the Ca(OH)₂-CO₂ Reaction. *Cryst. Growth Des.* **2016**, *16*(2), 728-736.

45
46
47
48 (27) Lee, T.; Tsai, Y. C.; Lee, H. L.; Lin, T. Y.; Chang, Y. H. Metal-Organic
49
50 Framework Engineering: Directed Assembly from Molecules to Spherical
51
52 Agglomerates. *J. Taiwan Inst. Chem. Eng.* **2016**, *62*, 10-20.

53
54
55
56 (28) Jarvis, L. M. The Year in New Drugs. *C&EN* **2014**, *92*(4), 10-13.

1
2
3
4
5 (29) Guzowski, J.; Kiesman, W.; Irdam, E. Process for Preparing High Purity and
6
7
8 Crystalline Dimethyl Fumarate. U.S. Patent 9422226 B2, August 23, 2016.
9

10 (30) Kooijman, H.; Sprengers, J. W.; Agerbeek, M. J.; Elsevier, C. J.; Spek, A. L.
11
12
13 Dimethyl Fumarate. *Acta Cryst.* **2004**, *E60*, o917-o918.
14

15 (31) Rönneck, R.; Salmi, T.; Vuori, A.; Haario, H.; Lehtonen, J.; Sundqvist, A.;
16
17
18 Tirronen, E. Development of a Kinetic Model for the Esterification of Acetic Acid
19
20
21 with Methanol in the Presence of a Homogeneous Acid Catalyst. *Chem. Eng. Sci.*
22
23
24
25 **1997**, *52*(19), 3369-3381.
26

27 (32) Lee, T.; Hsu, F. B. A Cross-Performance Relationship Between Carr's Index
28
29
30 and Dissolution Rate Constant: The Study of Acetaminophen Batches. *Drug Dev.*
31
32
33
34
35 *Ind. Pharm.* **2007**, *33*(11), 1273-1284.
36

37 (33) Lee, T.; Lin, H. Y.; Lee, H. L. Engineering Reaction and Crystallization and the
38
39
40 Impact on Filtration, Drying, and Dissolution Behaviors: The Study of
41
42
43 Acetaminophen (Paracetamol) by In-Process Controls. *Org. Process Res. Dev.* **2013**,
44
45
46
47 *17*(9), 1168-1178.
48

49 (34) Yadav, G. D.; Thathagar, M. B. Esterification of Maleic Acid with Ethanol
50
51
52 over Cation-Exchange Resin Catalysts. *React. Funct. Polym.* **2002**, *52*(2), 99-110.
53

54 (35) Lee, T.; Kuo, C. S.; Chen, Y. H. Solubility, Polymorphism, Crystallinity, and
55
56
57 Crystal Habit of Acetaminophen and Ibuprofen by Initial Solvent Screening. *Pharm.*
58
59

1
2
3
4
5
6
7
8
9
10
11
12
13
14
15
16
17
18
19
20
21
22
23
24
25
26
27
28
29
30
31
32
33
34
35
36
37
38
39
40
41
42
43
44
45
46
47
48
49
50
51
52
53
54
55
56
57
58
59
60

Technol. **2006**, *30* (10), 72-92.

(36) Lamas, J. P.; Sanchez-Prado, L.; Regueiro, J.; Llompert, M.; Garcia-Jares, C. Determination of Dimethyl Fumarate and Other Potential Allergens in Desiccant and Antimould Sachets. *Anal Bioanal Chem.* **2009**, *394*(8), 2231-2239.

(37) Lee, T.; Su, Y. C.; Hou, H. J.; Hsieh, H. Y. Spherical Crystallization for Lean Solid-Dose Manufacturing (Part I). *Pharm. Technol.* **2010**, *34*(3), 72-75.

(38) Tiong, N.; Elkordy, A. A. Effects of Liquisolid Formulations on Dissolution of Naproxen. *Eur. J. Pharm. Biopharm.* **2009**, *73*(3) 373-384.

(39) Guzowski, Jr., J. P.; Delaney, E. J.; Humora, M. J.; Irdam, E.; Kiesman, W. F.; Kwok, A.; Moran, A. D. Understanding and Control of Dimethyl Sulfate in a Manufacturing Process: Kinetic Modeling of a Fischer Esterification Catalyzed by H₂SO₄. *Org. Process Res. Dev.* **2012**, *16*(2), 232-239.

(40) Anderson, R. J.; Bendell, D. J.; Groundwater, P. W. Nuclear Magnetic Resonance Spectroscopy. In *Organic Spectroscopic Analysis*; Abel, E. W. Royal Society of Chemistry, Cambridge, 2004; pp.60-64.

(41) Blandin, A.-F.; Rivoire, A.; Mangin, D.; Klevin, J.-P.; Bossoutrot, J.-M. Using in Situ Image Analysis to Study the Kinetics of Agglomeration in Suspension. *Part. Part. Syst. Charact.* **2000**, *17*, 16-20.

(42) Thati, J.; Rasmuson, Å. C. On the Mechanisms of Formation of Spherical

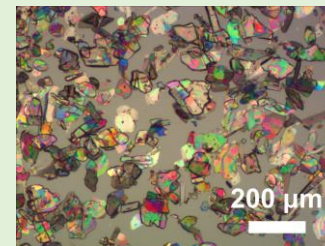
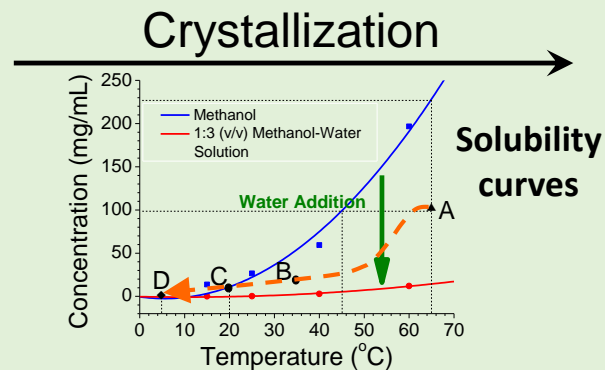
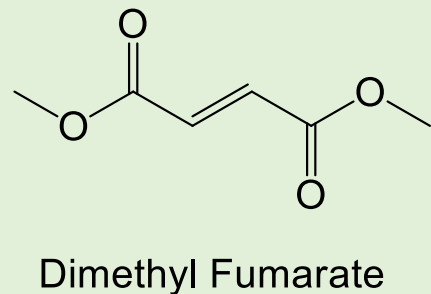
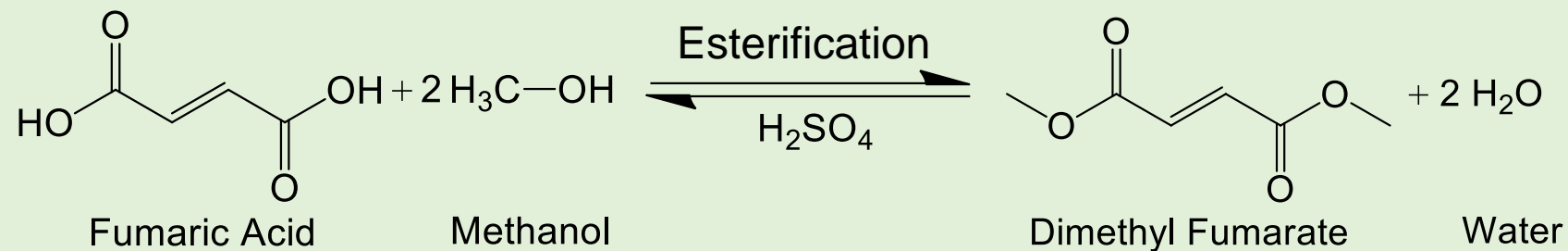
1
2
3
4
5 Agglomerates. *Eur. J. Pharm. Sci.* **2011**, *42*(4), 365-379.

6
7
8 (43) Thati, J.; Rasmuson, Å. C. Particle Engineering of Benzoic Acid by Spherical
9
10 Agglomeration. *Eur. J. Pharm. Sci.* **2012**, *45*(5), 657-667.

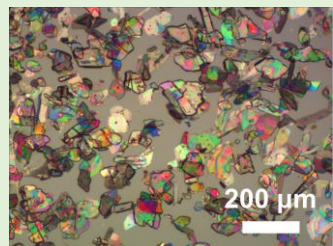
11
12
13 (44) Blandin, A. F.; Mangin, D.; Rivoire, A.; Klein, J. P.; Bossoutrot, J. M.
14
15 Agglomeration in Suspension of Salicylic Acid Fine Particles: Influence of Some
16
17 Process Parameters on Kinetics and Agglomerate Final Size. *Powder Technol.* **2003**,
18
19 *130*(1-3), 316-323.

20
21
22 (45) Nocent, M.; Bertocchi, L.; Espitalier, F.; Baron, M.; Couarraze, G. Definition
23
24 of a Solvent System for Spherical Crystallization of Salbutamol Sulfate by
25
26 Quasi-Emulsion Solvent Diffusion (QESD) Method. *J. Pharm. Sci.* **2001**, *90*(10),
27
28 1620-1627.

29
30
31 (46) Katta, J.; Rasmuson, Å. C. Spherical Crystallization of Benzoic Acid. *Inter. J.*
32
33 *Pharm.* **2008**, *348*(1-2), 61-69.
34
35
36
37
38
39
40
41
42
43
44
45
46
47
48
49
50
51
52
53
54
55
56
57
58
59
60

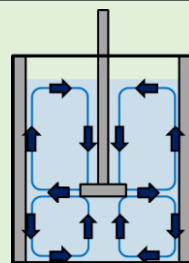


Primary crystals of dimethyl fumarate

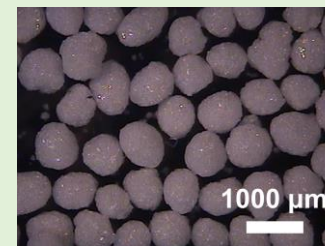


Primary crystals of dimethyl fumarate

Spherical Agglomeration



Agitation/
collision



Round granules of dimethyl fumarate

Three-in-One Intensified Process



Experimental setup